



ELSEVIER

Available online at [www.sciencedirect.com](http://www.sciencedirect.com)

SCIENCE @ DIRECT®

Computer Vision  
and Image  
Understanding

Computer Vision and Image Understanding 99 (2005) 58–95

[www.elsevier.com/locate/cviu](http://www.elsevier.com/locate/cviu)

## Focal length calibration from two views: method and analysis of singular cases

P. Sturm<sup>a</sup>, Z.L. Cheng<sup>b,\*</sup>, P.C.Y. Chen<sup>c,\*</sup>, A.N. Poo<sup>b</sup>

<sup>a</sup> INRIA Rhône-Alpes, 38330 Montbonnot, St. Martin, France

<sup>b</sup> Mechanical Engineering Department, National University of Singapore, 119260 Singapore, Singapore

<sup>c</sup> Bachelor of Technology Programme, Faculty of Engineering, National University of Singapore, 119260 Singapore, Singapore

Received 20 October 2003; accepted 1 November 2004

Available online 18 December 2004

---

### Abstract

We consider the problem of estimating the focal length of a camera from two views while the focal length is not varied during the motion of the camera. An approach based on Kruppa's equations is proposed. Specifically, we derive two linear and one quadratic equations to solve the problem. Although the three equations are interdependent in general, each one may be singular for different configurations. We study in detail the generic singularities of the problem and the actual singularities of the individual calibration equations. Results of our experiments using synthetic and real data underline the effect that singular configurations may have on self-calibration. However, these results are stable once the singularities are avoided.

© 2004 Elsevier Inc. All rights reserved.

*Keywords:* Camera calibration; Kruppa's equations; 3D reconstruction

---

\* Corresponding authors. Fax: +65 6777 3525 (P.C.Y. Chen).

E-mail addresses: [chengz@rpi.edu](mailto:chengz@rpi.edu) (Z.L. Cheng), [engchenp@nus.edu.sg](mailto:engchenp@nus.edu.sg) (P.C.Y. Chen).

<sup>1</sup> Present address: 23, 13th Street, 3rd floor, Troy, NY 12180, USA.

## 1. Introduction

Camera self-calibration has been studied for various scenarios. In the original scenario [3], the case of a camera with constant but completely unknown intrinsic parameters is considered. Since then, this has been extended to cases where all but one of the intrinsic parameters may be varying [16,12]. Reports on recent advances and general overviews of the topic can be found in [11,4].

In parallel to the proposition of new algorithms, research has been conducted on “critical motions,” where camera configurations or trajectories will render self-calibration impossible in theory and unstable in practice, see e.g. [1,13,14,18,19,21,23].

In this paper, we consider what may be the simplest self-calibration scenario: two views of an unknown static scene are taken by a camera with constant parameters, with the assumption that all intrinsic parameters except the focal length are known. Although very simple, we believe that this is a very useful scenario in practice. It has been shown that it is even possible to calibrate a *varying* focal length from two views [6]. Simple algorithms for this purpose were proposed in [1,2,15,16]. One of the drawbacks of this scenario is that the problem is unsolvable whenever the optical axes of the two views are coplanar [14,15,21], which is always approximately the case for stereo systems. Other less likely critical configurations are also described in [14,15,21].

In this paper, we show that the assumption of a *constant* focal length reduces the number of critical configurations. The generic critical configurations (which we will also refer to as *singularities* or *degeneracies*) of the problem are given: the problem is unsolvable whenever the optical axes of the two views are parallel or if they intersect at a finite point equidistant from both optical centers.

We show that two linear and one quadratic equations can be derived from the singular value decomposition (SVD) of the fundamental matrix. All critical configurations for the individual equations are then revealed in detail. Especially, it is shown that the quadratic equation degenerates only in the generic cases, or in some cases when the focal length is equal to  $\pm 1$ , whereas the linear equations’ critical configurations are the same as for the above problem of estimating a *varying* focal length.

We believe that such a study of critical configurations is important, since it indicates which configurations to avoid in general, and explains why certain algorithms may still fail (see e.g., a study on Kruppa equations [19]).

The performance of the calibration equations is evaluated using synthetic and real data. In both cases, we are interested in investigating the camera setups close to critical configurations. As for the real images, we show that, when the critical configurations are avoided, the results are of acceptable accuracy and stability.

This paper is an extended version of [20], and contains more experimental results and a more in-depth theoretical study.

*Organization.* The problem is formulated in Section 2 and the calibration equations are derived in Section 3. Generic and equation-specific singularities are summarized in Sections 4 and 5. Experimental results are provided in Section 6 and the paper is concluded in Section 7. The appendices contain all proofs for the equation-specific singularities, organized in several sections in a logical sequence.

*Notations.* In this paper, matrices are represented in sans serif font (e.g.,  $K$ ), vectors in bold face (e.g.,  $\mathbf{q}$ ), and scalars in italics. Coefficients of a matrix  $U$  (respectively, a vector  $\mathbf{v}$ ) are denoted by  $U_{ij}$  (respectively,  $v_i$ ). Equality of matrices or vectors, up to scale, is denoted by  $\sim$ . For any vector  $\mathbf{v}$ ,  $[\mathbf{v}]_{\times}$  represents the skew-symmetric matrix associated with the cross product, i.e.,  $\mathbf{v} \times \mathbf{w} = [\mathbf{v}]_{\times} \mathbf{w}$ . Transposition of a vector  $\mathbf{v}$  is denoted as  $\mathbf{v}^T$ , and the inverse of the transpose of a matrix  $A$  as  $A^{-T}$ . In complex equations, we often use the shorthand notations  $c_{\alpha} = \cos \alpha$ ,  $s_{\alpha} = \sin \alpha$ , and  $t_{\alpha} = \tan \alpha$ .

## 2. Problem formulation

Throughout this paper, we use perspective projection as the camera model, with the following intrinsic parameters: the focal length  $f$ , the aspect ratio  $\tau$ , and the principal point  $(u_0, v_0)$ . A 3D point  $\mathbf{Q}$  is projected to an image point  $\mathbf{q}$  via

$$\mathbf{q} \sim \mathbf{P}\mathbf{Q} \sim \mathbf{K}\mathbf{R}(\mathbf{I} - \mathbf{t})\mathbf{Q},$$

where the rotation matrix  $\mathbf{R}$  and the vector  $\mathbf{t}$  represent the camera's orientation and position, respectively. The calibration matrix  $\mathbf{K}$  is defined as

$$\mathbf{K} = \begin{pmatrix} \tau f & 0 & u_0 \\ 0 & f & v_0 \\ 0 & 0 & 1 \end{pmatrix}.$$

In the following, assume that two images of a static scene are available and that a projective reconstruction is possible or, equivalently, that the fundamental matrix can be computed. Without loss of generality, assume that the first camera is located at the origin and that its rotation matrix is the identity matrix. With  $\mathbf{R}$  and  $\mathbf{t}$  being the extrinsic and  $\mathbf{K}'$  the intrinsic parameters of the second camera, the fundamental matrix of two images is given by [11]

$$\mathbf{F} \sim \mathbf{K}'^{-T} \mathbf{R}[\mathbf{t}]_{\times} \mathbf{K}^{-1}.$$

We assume that the aspect ratio and the principal point are known for both images and that their focal lengths are identical. We can thus move from a completely uncalibrated space to a “semi-calibrated” one, by computing an intermediate between the fundamental matrix and the essential matrix ( $\mathbf{R}[\mathbf{t}]_{\times}$  in the above equation)

$$\mathbf{G} \sim \begin{pmatrix} \tau' & 0 & 0 \\ 0 & 1 & 0 \\ u'_0 & v'_0 & 1 \end{pmatrix} \mathbf{F} \begin{pmatrix} \tau & 0 & u_0 \\ 0 & 1 & v_0 \\ 0 & 0 & 1 \end{pmatrix} \sim \begin{pmatrix} 1 & 0 & 0 \\ 0 & 1 & 0 \\ 0 & 0 & f \end{pmatrix} \mathbf{R}[\mathbf{t}]_{\times} \begin{pmatrix} 1 & 0 & 0 \\ 0 & 1 & 0 \\ 0 & 0 & f \end{pmatrix}. \quad (1)$$

We call  $\mathbf{G}$  the *semi-calibrated fundamental matrix*.

### 3. Calibration equations

Let the singular value decomposition [5] of  $G$  be given by

$$G = U\Sigma V^T,$$

with  $\Sigma = \text{diag}(a, b, 0)$  being the diagonal matrix of singular values ( $a, b > 0$ ) and  $U$  and  $V$  orthogonal matrices. We denote by  $\mathbf{u}_i$  and  $\mathbf{v}_j$  the  $i$ th and  $j$ th column of  $U$  and  $V$ , respectively. Note that the second epipole  $\mathbf{e}'$  of  $G$  is its left null space, i.e.,  $\mathbf{e}' \sim \mathbf{u}_3$ . It can be shown [9,23] that Kruppa's equations can be reinterpreted by the following relationship in terms of fundamental matrix and the epipole:

$$G \begin{pmatrix} f^2 & 0 & 0 \\ 0 & f^2 & 0 \\ 0 & 0 & 1 \end{pmatrix} G^T \sim [\mathbf{e}']_{\times} \begin{pmatrix} f^2 & 0 & 0 \\ 0 & f^2 & 0 \\ 0 & 0 & 1 \end{pmatrix} [\mathbf{e}']_{\times}.$$

In terms of the SVD of  $G$ , this can be written as

$$U\Sigma V^T \begin{pmatrix} f^2 & 0 & 0 \\ 0 & f^2 & 0 \\ 0 & 0 & 1 \end{pmatrix} V\Sigma U^T \sim [\mathbf{u}_3]_{\times} \begin{pmatrix} f^2 & 0 & 0 \\ 0 & f^2 & 0 \\ 0 & 0 & 1 \end{pmatrix} [\mathbf{u}_3]_{\times}.$$

Multiplying the equation by  $U^T$  from the left and  $U$  from the right gives, due to the orthogonality of  $U$

$$\begin{aligned} \Sigma V^T \begin{pmatrix} f^2 & 0 & 0 \\ 0 & f^2 & 0 \\ 0 & 0 & 1 \end{pmatrix} V\Sigma &\sim \begin{pmatrix} \mathbf{u}_1^T \\ \mathbf{u}_2^T \\ \mathbf{u}_3^T \end{pmatrix} [\mathbf{u}_3]_{\times} \begin{pmatrix} f^2 & 0 & 0 \\ 0 & f^2 & 0 \\ 0 & 0 & 1 \end{pmatrix} [\mathbf{u}_3]_{\times} (\mathbf{u}_1 \quad \mathbf{u}_2 \quad \mathbf{u}_3) \\ &\sim \begin{pmatrix} \mathbf{u}_2^T \\ -\mathbf{u}_1^T \\ \mathbf{0}^T \end{pmatrix} \begin{pmatrix} f^2 & 0 & 0 \\ 0 & f^2 & 0 \\ 0 & 0 & 1 \end{pmatrix} (\mathbf{u}_2 \quad -\mathbf{u}_1 \quad \mathbf{0}). \end{aligned}$$

The last row and the last column of this matrix equation are zero vectors, so we concentrate on the upper left  $2 \times 2$  part of the equation

$$\begin{pmatrix} a\mathbf{v}_1^T \\ b\mathbf{v}_2^T \end{pmatrix} \begin{pmatrix} f^2 & 0 & 0 \\ 0 & f^2 & 0 \\ 0 & 0 & 1 \end{pmatrix} (a\mathbf{v}_1 \quad b\mathbf{v}_2) \sim \begin{pmatrix} \mathbf{u}_2^T \\ -\mathbf{u}_1^T \end{pmatrix} \begin{pmatrix} f^2 & 0 & 0 \\ 0 & f^2 & 0 \\ 0 & 0 & 1 \end{pmatrix} (\mathbf{u}_2 \quad -\mathbf{u}_1).$$

Making use of the fact that the vectors  $\mathbf{v}_1$ , etc., have unit norm, we can further simplify the above equation to obtain

$$\begin{aligned} &\begin{pmatrix} a^2(f^2 + V_{31}^2(1 - f^2)) & abV_{31}V_{32}(1 - f^2) \\ abV_{31}V_{32}(1 - f^2) & b^2(f^2 + V_{32}^2(1 - f^2)) \end{pmatrix} \\ &\sim \begin{pmatrix} f^2 + U_{32}^2(1 - f^2) & -U_{31}U_{32}(1 - f^2) \\ -U_{31}U_{32}(1 - f^2) & f^2 + U_{31}^2(1 - f^2) \end{pmatrix}. \end{aligned}$$

The equality (up to scale) of these two symmetric matrices gives rise to three individual quadratic equations in  $f^2$  (by forming the cross-product of the vectors containing the three different coefficients of each matrix). Two of these have the trivial solution<sup>2</sup>  $f^2 = 1$ . Factoring this out, we thus obtain two linear equations and a quadratic one:

$$f^2 \{ aU_{31}U_{32}(1 - V_{31}^2) + bV_{31}V_{32}(1 - U_{32}^2) \} + U_{32}V_{31}(aU_{31}V_{31} + bU_{32}V_{32}) = 0, \quad (2)$$

$$f^2 \{ aV_{31}V_{32}(1 - U_{31}^2) + bU_{31}U_{32}(1 - V_{32}^2) \} + U_{31}V_{32}(aU_{31}V_{31} + bU_{32}V_{32}) = 0, \quad (3)$$

$$\begin{aligned} & f^4 \{ a^2(1 - U_{31}^2)(1 - V_{31}^2) - b^2(1 - U_{32}^2)(1 - V_{32}^2) \} \\ & + f^2 \{ a^2(U_{31}^2 + V_{31}^2 - 2U_{31}^2V_{31}^2) - b^2(U_{32}^2 + V_{32}^2 - 2U_{32}^2V_{32}^2) \} \\ & + \{ a^2U_{31}^2V_{31}^2 - b^2U_{32}^2V_{32}^2 \} = 0. \end{aligned} \quad (4)$$

These are our self-calibration equations. They are of course algebraically dependent, but we will see in the following sections that they may be singular in different conditions.

### 3.1. Calibration algorithm

A simple calibration algorithm can be formulated as follows:

- (1) Estimate the fundamental matrix between the two views (algorithms with good performance are given in [22]).
- (2) “Undo” the known intrinsic parameters, as shown in Eq. (1).
- (3) Compute the SVD of  $G$  and extract the coefficients  $U_{31}$ ,  $U_{32}$ ,  $V_{31}$ , and  $V_{32}$ , as well as the non-zero singular values  $a$  and  $b$ .
- (4) Construct and solve any of the Eqs. (2)–(4). In practice, we only solve the quadratic equation. The spurious solution can either be ruled out using the linear equations, or usually by simply taking the solution closest to a reasonable guess (in simulations, the spurious solution was always observed to be far off the true one).
- (5) Optionally, the result can be improved by bundle adjustment, after having estimated the relative pose of the cameras.

### 3.2. On standardization

It is often advisable to work in “standardized” image coordinates [8], which is usually achieved by translating and scaling image coordinates appropriately. The transformation applied in step (2) of the above algorithm, mainly amounts to such

<sup>2</sup> The case where the true squared focal length equals 1, is discussed in Appendix D; this might occur if working in standardized coordinates.

a translation, and one might also apply an additional scaling. Usually, the range of feasible focal lengths is well known, and one might apply a scaling with the inverse of a feasible focal length value  $f_0$  (standardization based on image point coordinates as in [8] amounts usually to such a scaling). The semi-calibrated fundamental matrix would be transformed according to

$$\begin{pmatrix} f_0 & 0 & 0 \\ 0 & f_0 & 0 \\ 0 & 0 & 1 \end{pmatrix} G \begin{pmatrix} f_0 & 0 & 0 \\ 0 & f_0 & 0 \\ 0 & 0 & 1 \end{pmatrix}. \quad (5)$$

The rest of the algorithm will be the same, except that the estimated focal length, has to be multiplied by  $f_0$  at the end.

In Section 5 and in the appendix, we show that if  $f_0$  happens to be equal to the true focal length, then the calibration equations may become degenerate. Thus, with  $f_0$  close to the true focal length, one may expect an instable focal length estimation. In Section 6.1.4, this is shown to occur in some situations. On the other hand, when applying no such scaling, instabilities were observed in other situations. A rule of thumb that we apply in practice is thus to apply a scaling by a value  $f_0$  significantly larger than the maximum expected focal length. This (admittedly ad hoc) procedure gave always good performance.

#### 4. Generic singularities

Before discussing singularities associated with the above calibration equations, we describe the generic singularities of the underlying problem, i.e., those that cannot be overcome by *any* algorithm. They can be obtained rather directly by specializing the results obtained for *varying* focal lengths [14,15,17,21].

The only critical configurations for the (self-) calibration of a constant focal length from two views are:

- the optical axes are parallel to each other, or
- the optical axes intersect at a finite point and the optical centers are equidistant from this point. We refer to this configuration as the *equidistance configuration*. We may consider that it subsumes the case of parallel optical axes: although the optical axes intersect at a point at infinity, we may consider that the intersection point is equidistant from the optical centers (at infinite distance).

In both these cases, there is an infinite number of solutions for  $f^2$ .

Kahl and Triggs [13] have derived critical configurations. However, their results are not as clearly stated as above, and seem slightly incomplete. For example, their “turntable” rotation about the intersection point of the optical axes cannot produce all possible cyclotorsions of the two cameras, i.e., rotations about

their optical axes (which do not affect the self-calibration problem discussed in this paper).

Coplanarity of the optical axes is a necessary condition for a singular configuration with *equal* focal lengths, whereas it is already sufficient if two *different* focal lengths have to be estimated [14,15,17,21]. We will see in the following section that the quadratic Eq. (4) is nearly only degenerate in the generic singular cases (with the exception of  $f = \pm 1$ ). On the other hand, the linear equations are degenerate when the two optical axes are coplanar, and in a particular case of little practical importance.

The stability of calibration in near-degenerate situations should be better for the equal focal length case.

## 5. Singularities of the calibration equations

It is useful to examine the singularities of the above calibration equations. Here we will determine under what conditions the individual equations become singular. This will allow us to see if they suffer from non-generic singularities and possibly to determine which equation to use under what condition, or to determine a single equation that should always be used.

The equations are said to be singular if they lead to invalid solutions. Such solutions may arise when there is an infinite number of choices for the coefficients of the equations' unknowns, or when the coefficients are equal to zero. If the SVD of  $G$  is unique (up to sign or swapping the columns of  $U$  and  $V$  and corresponding singular values), the forms of (4), (2), and (3) are unique. Otherwise, there may be invalid solutions. In the absence of noise, the true squared focal length is necessarily a solution of the equations. For the quadratic equation, there is in general a second, spurious solution. In most cases, this is a negative value and can thus be discarded (since we are looking for the *squared* focal length). In some cases, however, the equations may have an infinite number of solutions: for certain singular *relative camera poses*, all coefficients of our polynomial equations vanish, implying an infinite number of solutions for  $f$ . In the following, all singular *relative camera poses* are summarized. Proofs for the following statements are given in the appendices.

All three equations vanish of course in the generic singular conditions given in Section 4, i.e., their coefficients all become zero here. For the quadratic equation, there are, in general, no further singularities (unlike the general Kruppa equations that are subject to non-generic singularities). The only exception occurs when the true focal length equals  $\pm 1$ , which means that the semi-calibrated fundamental matrix is a fully calibrated fundamental matrix, i.e., an essential matrix. This can happen if the fundamental matrix is expressed in perfectly standardized coordinates, meaning that the coordinate scaling recommended in [8] happens to be done by the inverse of the focal length. The essential matrix has two equal non-zero singular values, which means that its SVD is not unique: there is a one-degree-of-freedom family of possible SVDs. It is shown in Appendix D.2 that, depending on which

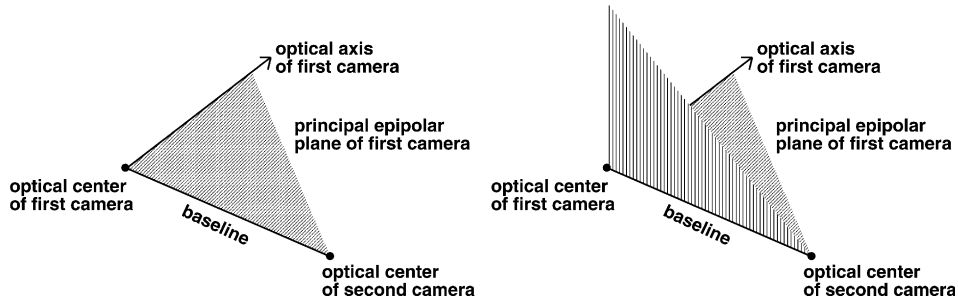


Fig. 1. Example of a singular case for the linear equations when the optical axes are not coplanar. (Left) The notion of principal epipolar plane is illustrated (plane spanned by the optical centers and one optical axis). (Right) If the optical axis of the second camera lies anywhere in the plane  $\Pi$ , which is orthogonal to the first camera's principal epipolar plane, then the linear equations become degenerate. In that case the two principal epipolar planes are orthogonal to one another (unless the optical axis points towards the first camera's optical center, in which case the principal epipolar plane of the second camera is not defined).

of the ambiguous SVDs one happens to compute in practice,<sup>3</sup> the quadratic equation's coefficients may vanish, even for a camera configuration that is generically non-singular. We show in Appendix D.2 that only a finite number, among the infinite number of possible SVDs, cause such a singularity. It is thus unlikely to encounter exactly such a case. However, when working in standardized coordinates (or, when scaling with approximately the true inverse focal length), one may get close enough, in which case noise in the data may create instabilities. This effect is studied using simulations, cf. Section 6.1.4, and conclusions are stated above in Section 3.2.

For the linear equations, there is degeneracy in two cases. The first case is when the optical axes are coplanar. The other case is best explained as follows. The family of epipolar planes consists of the pencil of planes that contain the cameras' baseline, i.e., the line joining the two optical centers. We define a *principal epipolar plane* associated with a camera as the epipolar plane that contains its optical axis, cf. the left part of Fig. 1. This is uniquely defined unless the optical axis coincides with the baseline, in which case, at least one camera looks straight at the other one. The non-generic singularities of the two linear calibration equations can be described, using the principal epipolar planes of the two cameras, in the following scenarios:

- Neither of the two principal epipolar planes is uniquely defined. This means that the two optical axes are identical, which implies of course that they are parallel (and coplanar). This is a generic singular case, and naturally all three equations become degenerate.
- One of the principal epipolar planes is not uniquely defined. This is a special case of coplanar optical axes. The linear equations degenerate, whereas the quadratic one does not in general.

<sup>3</sup> This depends on the implementation used for SVD computation and the outcome is possibly non-deterministic.

- The principal epipolar planes are identical. This means that the optical axes are coplanar. The linear equations degenerate. The quadratic equation degenerates only if, in addition, the equidistance configuration is present. Otherwise, its spurious solution is always zero (cf. Section E.3), i.e., the true solution can be obtained without ambiguity.
- The principal epipolar planes are orthogonal to each other. In this case, the linear equations degenerate. The quadratic equation does not degenerate, and its spurious solution is always negative or zero (cf. Section F.2), i.e., the true solution can be obtained without ambiguity. This situation is illustrated in the right part of Fig. 1.

*Summary.* The quadratic equation is degenerate practically only in generic singular configurations. In addition, whenever the linear equations degenerate in generic non-singular configurations, the quadratic one gives a unique admissible solution for the squared focal length.

It is interesting to note that the non-generic singularities for the linear equations (coplanar optical axes and orthogonal principal epipolar planes) correspond to generic singular camera configurations for the case of *different* focal lengths [14,15,17,21].

## 6. Experimental results

We conducted various experiments with our algorithm, to evaluate its performance with respect to several factors. Specifically, we studied its behavior in the proximity of singular configurations. This was done systematically using both simulated data and real data to give some intuition on how much effort has to be spent in avoiding singularities in practice. We also evaluated the performance with respect to the level of noise in the data and with respect to errors in the assumption of the location of the principal point. Experiments with real images were carried out for images of a calibration grid and also for images of a few generic scenes.

### 6.1. Simulated data

We conducted simulated experiments to assess the sensitivity of the calibration equations in close-to-singular situations. Fig. 2 shows the simulated scenarios. The starting position of the cameras is depicted on the left. It is the typical stereo situation, with symmetric vergence angles  $\alpha$ . This situation is singular: the optical axes are coplanar and the optical centers are equidistant from the intersection point of the optical axes.

In the first scenario, the second camera rotates away from the plane spanned by the initial position of the optical axes, by an angle between  $0^\circ$  and  $5^\circ$  (“elevation angle”). In Fig. 2, this rotation would be towards the reader.

In the second scenario (shown on the right of Fig. 2), the second camera moves along its optical axis. The optical axes stay coplanar, but the distances of the optical centers to the intersection point of the optical axes are no longer equal. Hence, the

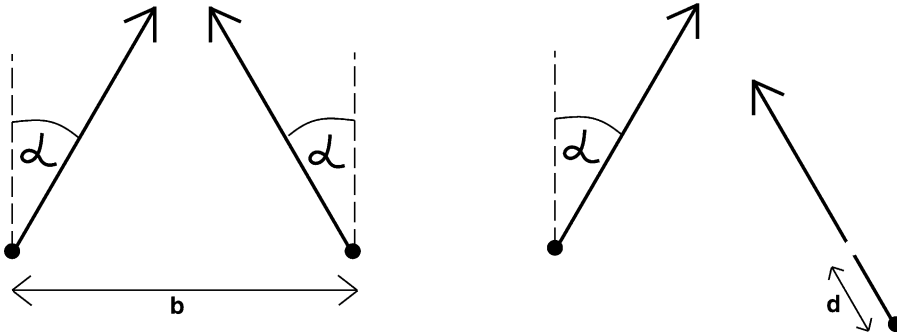


Fig. 2. Simulation scenarios. Shown are the optical centers and optical axes. (Left) Initial camera pose;  $b$  is the distance between the optical centers and  $\alpha$  the vergence angle of the optical axes. (Right) Second simulation scenario; the second camera is moved along its optical axis by the distance  $d$ .

scenario is not singular any more (generically, and for the quadratic equation), besides for the case of a zero vergence angle (parallel optical axes). The baseline of the system is  $b = 1000$  U, and the displacement of the second camera is by  $d = -250, -200, \dots, 250$  U.

For both scenarios, experiments are done with different vergence angles, with  $\alpha$  between  $0^\circ$  (parallel optical axes in the initial position) and  $30^\circ$ . Three dimensional scene points are created randomly as follows: their coordinates are drawn from a uniform distribution inside a rectangular volume in front of the cameras, whose depth is 10 times the baseline. Only points inside the field of view of both cameras are used. Cameras are simulated with a focal length of 1000 pixels and a field of view of  $28.7^\circ$ , corresponding to images of size  $512 \times 512$ . By default, 100 points are used in each experiment, unless otherwise stated. The 3D points are projected to the images, and centered Gaussian noise (with a standard deviation between 0 and 1 pixels), is added to the image point coordinates. These image points are the input to the algorithm.

The following figures show mainly results for the quadratic equation. Results for the linear equations are not shown here, however, they are discussed in the text. Displayed are the median values of the relative errors on the focal length (ratio of the difference between true and estimated focal length, and the true focal length); each data point in the graphs is the result of 1000 random experiments. In all simulated experiments, the 8-point method of [8] is used to compute the fundamental matrix, i.e., no non-linear optimization was done.

#### 6.1.1. First scenario: off-plane rotation

Fig. 3 shows results for this scenario. The upper left part is relative to a zero vergence angle (i.e., with an elevation angle of  $0^\circ$ , the optical axes are parallel and the configuration is singular), and the upper right part is relative to a vergence angle of  $5^\circ$ . For zero vergence, it can be seen that even for a  $3^\circ$  rotation off the base plane, the errors are below 10% for realistic noise levels. Slight vergence of the cameras significantly improves the results (compare the upper right with the upper left part of Fig. 3).

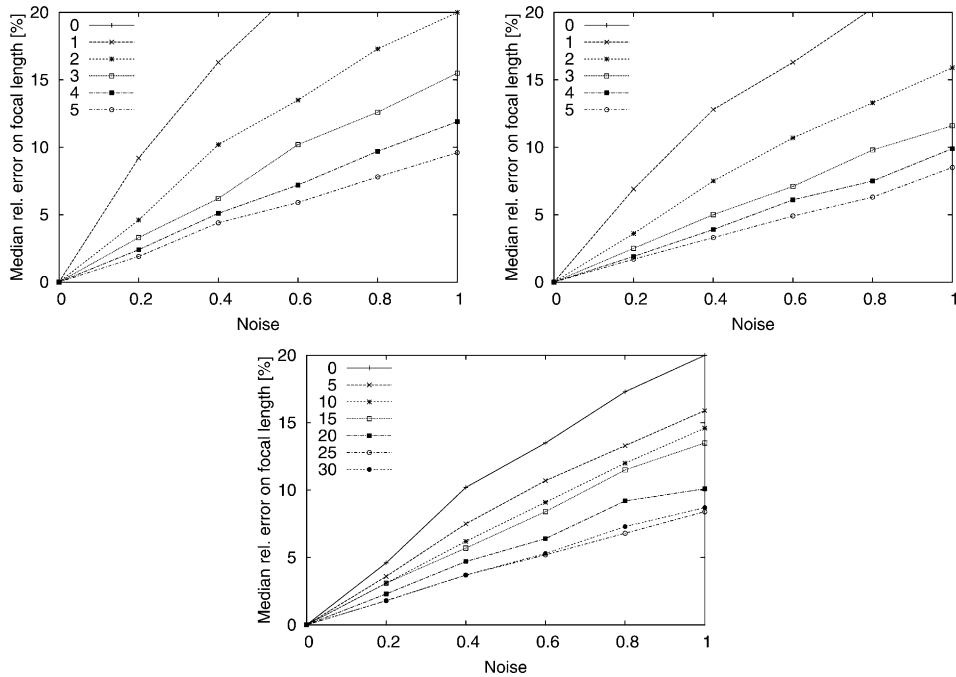


Fig. 3. First scenario. (Top) Results are shown for different elevation angles (one curve per elevation angle, from  $0^\circ$  to  $5^\circ$ , cf. the graphs' legends). The curves for  $0^\circ$  elevation are outside the graphs (this situation is singular, and the results reflect this). (Upper left) Vergence fixed to  $0^\circ$ . (Upper right) Vergence fixed to  $5^\circ$ . (Bottom) Elevation angle fixed to  $2^\circ$ , results shown for different vergence angles (one curve per vergence angle,  $0^\circ$ ,  $5^\circ$ , ...,  $30^\circ$ , cf. legend).

In the lower part of Fig. 3, the elevation angle is kept fixed to  $2^\circ$ , to illustrate the influence of the vergence angle  $\alpha$ . It is intuitive that with a vergence angle of  $0^\circ$ , the configuration is “closer” to the degenerate situation of parallel optical axes, thus the focal length estimation less stable, compared to larger vergence angles. This is reflected in the graph: the error in the estimated focal length decreases with increasing vergence angle, although above  $25^\circ$  vergence, there is no further significant improvement.

It is worthy to note that the linear equations gave nearly identical results to the quadratic one in this scenario. Since two linear equations are available, the average of their results is taken as estimated focal length, unless one of the two gave a negative solution for  $f^2$ , in which case only the solution of the other equation was used of course.

#### 6.1.2. Second scenario: displacement of the second camera

Fig. 4 shows results for the second scenario. The upper part of the figure shows the influence of the vergence angle for a fixed, relatively small displacement (5% of the baseline) of the second camera. For a vergence angle of  $0^\circ$ , the optical axes

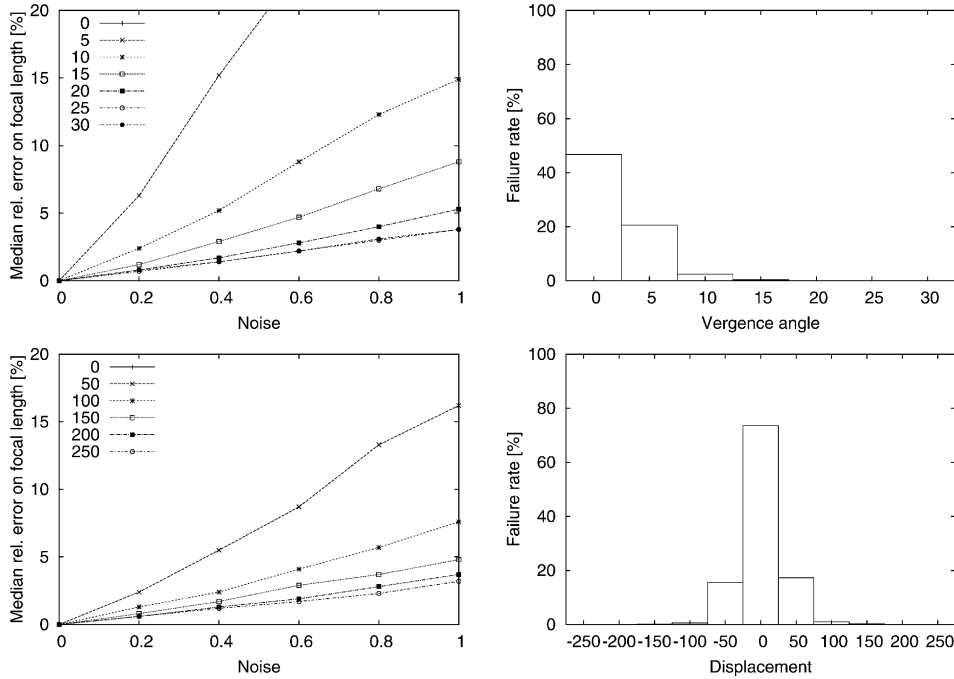


Fig. 4. Second scenario. (Top) Fixed displacement  $d = -50$ . (Upper left) Relative errors on estimated focal length for different vergence angles. (Upper right) Failure rates (see text) for a noise level of 0.6 pixels and different vergence angles. (Bottom) Fixed vergence angle of  $10^\circ$ . (Lower left) Relative errors on estimated focal length for different displacements (for  $d = 0, 50, \dots, 250$  U, cf. graph's legend). (Lower right) Failure rates for a noise level of 1 pixel.

are parallel and the situation remains singular for any displacement, which is reflected by the fact that the corresponding curve is outside the graph. The figure shows that close to  $0^\circ$  vergence, the results are heavily affected by the near-singularity and noise, but they stabilize with increasing vergence angle. This is shown by the error on the focal length, which decreases significantly with increasing vergence angle (upper left part of Fig. 4), as well as by the decreasing failure rate (upper right). Failure was declared whenever the quadratic equation did not admit a positive solution.

The lower part of Fig. 4 shows the results with respect to varying displacement, for a fixed vergence angle of  $10^\circ$ . The curve for zero displacement is outside the graph (this corresponds to the singular equidistance configuration). With increasing displacement, the performance increases as expected, both in terms of relative error on the estimated focal length and failure rate. The graphs for displacements towards the scene (negative  $d$ ) are not plotted in the lower left part of Fig. 4, for the sake of clarity; note that the graph for a value of  $-d$  is very similar to that for  $d$ .

As for the linear equations, this scenario is singular (coplanar optical axes). This is reflected by experimental results (not shown here), where relative errors are sometimes above 100%, and nearly always above 70% (besides a high failure rate).

### 6.1.3. Influence of the number of point correspondences

In Fig. 5, we show results on the influence of the number of point correspondences used for computing the fundamental matrix. As expected, performance increases with the number of points, with an asymptotic behavior.

### 6.1.4. Influence of standardization

As discussed in Sections 3.2 and 5, the use of standardized coordinates (in our case, a scaling) has to be considered more closely. Here, we show results obtained with different scalings. The  $x$ -axis of the graphs in Figs. 6 and 7 shows the inverse scale factor applied to the fundamental matrix according to Eq. (5) (remember that the true focal length is 1000). The graphs show the percentage of random experiments where the focal length was estimated (positive solution for  $f^2$ ) and was within 10% of the ground truth value. Results are shown for both, quadratic and linear equations.

Fig. 6 shows results for the first scenario. All graphs show a clear “performance hole” when scaling is done with a factor close to the actual inverse focal length. With decreasing elevation angle (bottom to top) and increasing noise (left to right), the instability caused by scaling with the inverse focal length, gets combined with the increasing instability due to getting closer to the singular equidistance case. In the least favorable case (upper right), the success rate drops to an average of around 30%. Overall, the linear equations are much more sensitive to the scale factor, compared to the quadratic equation, which has close to 100% success in the favorable case on the lower left, even when scaling is done with approximately the true inverse focal length.

Fig. 7 shows results for the second scenario. The linear equation is degenerate here, and the results are always bad, as stated in Section 6.1.2. As for the quadratic equation, the same performance hole as above around the true focal length can be observed. Interestingly, performance also drops significantly for scale factors below 50 (extreme left side of the graphs); the only explanation we can think of is that in this special case, round-off error becomes too large.

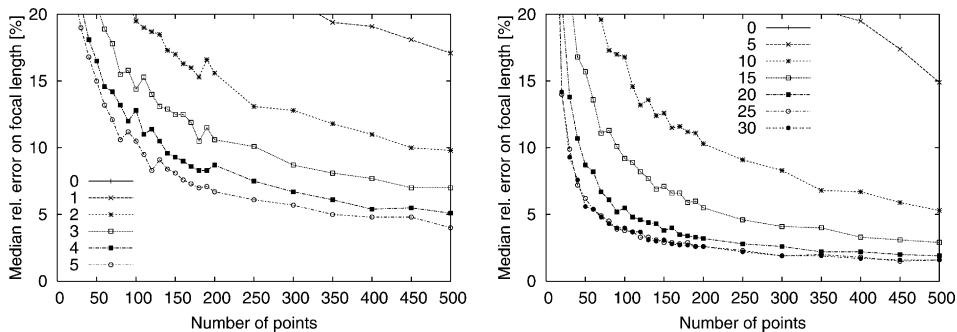


Fig. 5. (Left) First scenario (cf. Section 6.1.1), vergence fixed to  $0^\circ$ , noise level of 1 pixel, results for different elevation angles. (Right) Second scenario (cf. Section 6.1.2), displacement of  $-50$ , noise level of 1 pixel, results for different vergence angles.

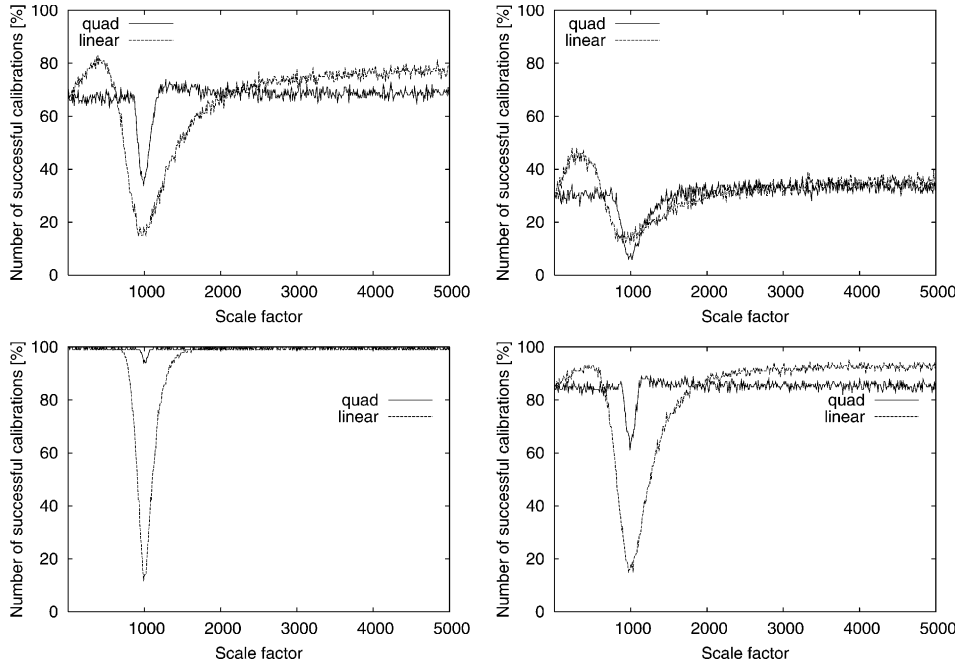


Fig. 6. First scenario, with vergence fixed to  $30^\circ$ . (Top) Elevation angle fixed to  $1^\circ$ . (Bottom) Elevation angle fixed to  $5^\circ$ . (Left column) Noise level of 0.4 pixels. (Right column) Noise level of 1 pixel.

Based on these observations, we decided to scale by a factor much lower than the inverse of the maximum expected focal length, as stated already in Section 3.2. In all other simulated experiments, a scale factor of  $1/5000$  was thus used, which always gave good results.

## 6.2. Real images of a calibration grid

Using real images of a calibration grid, we attempted to evaluate the algorithm's performance with respect to proximity to singular configurations and its sensitivity to the assumption of the principal point's position.

### 6.2.1. Experimental setup

It is relatively easy to avoid singular configurations in practice. Especially, one should avoid the case of coplanar optical axes. There are multiple ways to achieve this goal. One approach is as follows. Before taking the second image, point the camera to the same point in the scene as in the first image (this is simple to do with a viewfinder). Then, tilt the camera slightly upwards or downwards, and take the second image. Determining by how much one should tilt the camera is one of the goals of this experiment.

We took a total of 10 images of a calibration grid with a handheld camera. Fig. 8 shows some sample images. They were taken from 10 different positions, covering a

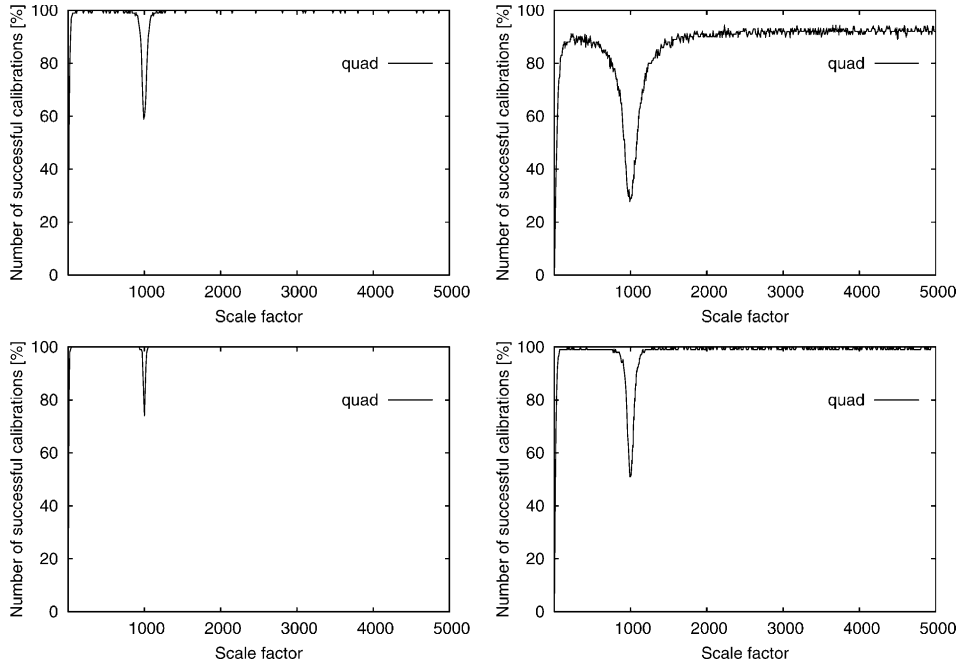


Fig. 7. Second scenario, with vergence fixed to  $30^\circ$ . (Top) Displacement of  $-50$ . (Bottom) Displacement of  $-100$ . (Left) Noise level of 0.4 pixels. (Right) Noise level of 1 pixel.



Fig. 8. Some images of the calibration grid.

roughly circular path around the grid (i.e., most pairs of views are close to the singular equidistance configuration, cf. Section 4). From each position, we applied a small tilt angle and then took one image as described above. Thus, among the 45 possible image pairs, some have approximately coplanar optical axes while some do not.

For this experiment and the ones in the next section, we used a Sony DSC-P31 digital camera with 5 mm focal length and chose a moderate image resolution of  $640 \times 480$ .

The camera was calibrated, including radial lens distortion, using all 10 images of the grid, by a photogrammetric calibration algorithm. The resulting focal length of

625 pixels is used as “ground truth” in the following experiments. The images were corrected for distortion before applying our algorithm. The extracted image positions of the grid’s targets were used by our algorithm to compute the fundamental matrix.

### 6.2.2. Effect of principal point estimation on focal length calibration

As described above, our focal length calibration algorithm is based on the assumption that we know the other intrinsic parameters. Here, we show that an error on the assumed location of the principal point has little effect on the computed focal length. For one pair of images, we estimated the focal length repeatedly, changing (in steps of 5 pixels) the assumed coordinates of the principal point by up to  $\pm 25$  pixels from the image center in both directions.

Among the 121 different computed focal lengths, the maximum relative error with respect to the true focal length was 4.16%. The mean relative error was 0.2%. The standard deviation of the computed focal lengths was 11.7 pixels, i.e., only about 1.8% of the focal length. We conclude that realistic errors in the assumption of the principal point’s position have little effect on our algorithm, at least concerning the range of accuracy that one can expect in our minimal scenario. Hence it is usually safe to assume that the principal point is at the image center when we use this algorithm for focal length calibration.

### 6.2.3. Stability of the algorithm

Here, we evaluate the algorithm’s performance, with respect to how close the optical axes are to being coplanar. The calibration of our images, using a photogrammetric approach that makes use of the known geometry of the calibration grid, tells us the position of the optical centers and the optical axes for our 10 images. To measure how close the optical axes associated with two images are to being coplanar, we proceed as illustrated in the left part of Fig. 9: we compute the two principal epipolar planes  $p_1$  and  $p_2$  (cf. Section 5). The “middle plane” is the plane that “bisects”  $p_1$  and  $p_2$ . The angle  $c$  between the middle plane and  $p_1$  (or, equivalently,  $p_2$ ) is our measure for the deviation from the case of coplanar optical axes. In addition, we also considered a measure for how close the two optical axes are from being parallel, but which was found to be less significant for the following evaluation.

We applied our algorithm to all 45 possible image pairs formed by our 10 input images. The estimated values of the focal length are plotted in the right part of Fig. 9, over the value of the angle  $c$  for the corresponding image pair.

We observe three groups of results:

- For  $c > 1.5^\circ$ , the calibrated focal lengths are quite precise and accurate. Their average is 627.6, which is nearly identical to the ground truth. Their standard deviation is about 6.5 pixels, i.e., about 1.1% of the focal length.
- For  $c < 1^\circ$ , the results are not at all stable. Errors range from 25 to 280 pixels.
- For  $1^\circ < c < 1.5^\circ$ , the results are not very precise but become reasonably accurate.

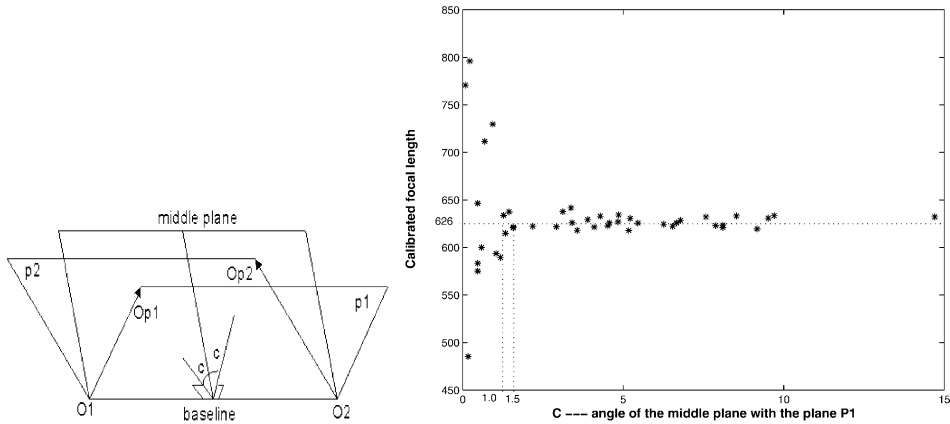


Fig. 9. (Left) The angle  $c$  used for measuring by how much an image pair deviates from having coplanar optical axes. (Right) Sensitivity of focal length with respect to the angle  $c$ .

We conclude that for the type of images tested, it is safe to run our algorithm whenever the angle  $c$  exceeds  $1.5^\circ$ . This corresponds to tilting the camera between two image acquisitions by about 10% of its opening angle, which seems to be reasonably achievable in practice. However, with a lower accuracy in image point extraction, this value will increase. In Section 6.3, we thus test our algorithm with real images of generic scenes.

#### 6.2.4. 3D reconstruction results using the calibrated focal length

Having calibrated the focal length, we can estimate the relative position of the two considered images [11] and carry out a 3D reconstruction of the matched image points [10]. We did this for several image pairs. To evaluate the quality of the 3D reconstruction, we compare it to the known geometry of the calibration grid. We take two steps to achieve this objective. First, we fit planes to the three subsets of coplanar points (cf. Fig. 8). Here, we design a relative distance to evaluate the coplanarity of points. Specifically, we first measure the distances of points to the fitted plane. Next, we compute the largest distance between pairs of the considered points. The distances of the points to the plane are then normalized by this largest distance. The obtained distances (in percent) are the so-called relative distances. Second, we measure the angles between each pair of planes and compare it to the “ground truth”: one of the grid’s planes forms  $90^\circ$  angles with the two others, which themselves form a  $120^\circ$  angle.

The results of our evaluation are displayed in Table 1. They are shown for five pairs, which share one common image. Note that from left to right, the baseline (the distance between optical centers) decreases. Row  $f$  contains the calibrated focal lengths. The rows  $A_{ij}$  (with  $i, j \in [1, 2, 3]$ ) show the angles between pairs of planes. The rows  $\text{Std}_i$  (with  $i \in [1, 2, 3]$ ) show, for the 3 planes, the standard deviation of the

Table 1  
Reconstruction results using calibrated focal length

	Ground truth	Pair 1	Pair 2	Pair 3	Pair 4	Pair 5
$f$	625.0	622.3	633.0	632.0	628.4	623.6
A12	90.0	90.17	89.75	91.12	90.49	89.89
A13	90.0	89.65	89.34	92.18	91.36	88.87
A23	120.0	119.79	119.88	120.32	120.57	118.56
Std1	0.0	1.3e−4	1.7e−4	2.4e−4	3.1e−4	3.2e−4
Std2	0.0	3.4e−4	3.5e−4	2.6e−4	3.8e−4	2.8e−4
Std3	0.0	2.8e−4	3.1e−4	4.9e−4	5.3e−4	3.8e−4

relative distances as described above, which is useful to evaluate the coplanarity of points.

We observe that for the two image pairs with the largest baselines, the angles are all within  $0.3^\circ$  from their true values. With decreasing baseline, the errors generally increase, both for the angles and the coplanarity measure, although they still stay relatively small.

### 6.3. Real images of generic scenes

For the images of the calibration grid, image point matching was provided due to the easy identification of the targets. Here, we consider images of two generic scenes. Interest point extraction and matching is done automatically using the available software<sup>4</sup> (see also [22]). The same camera zoom setting as in Section 6.2 was used, which provides the “ground truth” value for the focal length in Tables 2 and 3.

#### 6.3.1. An outdoor scene

We took five images of a building of the National University of Singapore (see Fig. 10, for examples). The distance between the camera and the building is about 25 m. The results for several image pairs are presented in Table 2 (camera configurations close to the coplanar case give poor results which are not shown here). After calibration, we also reconstructed the building. We chose the median of the seven calibrated results as shown in Table 2, and used the result to reconstruct the building’s two faces with the right angle. We found that the reconstructed results (about  $85^\circ$ ) are roughly close to the ground truth (the relative error is about 5%).

When analyzing the results of Table 2, we need to consider the following issue. Although the same zoom setting was used as for the images of the calibration grid, the camera focused on a scene at a different distance. Hence, comparatively large relative errors of several percent may be expected. Here, the maximum relative error is about 10%, which seems reasonable for this experiment.

<sup>4</sup> <http://www-sop.inria.fr/robotvis/personnel/~zzhang/software.html>.

Table 2  
Results for image pairs of the building, cf. Fig. 10

Image pair	Ground truth	12	14	15	23	25	34	35
$f$	625.0	643.2	654.3	604.7	688.6	689.8	592.4	657.7

The label “12” in the first row stands for the pair of images 1 and 2, and analogously for the other labels.

Table 3  
Results for image pairs of the 3 cups, cf. Fig. 11

Image pair	Ground truth	12	13	14	23	24	34
$f$	625.0	602.4	604.8	596.9	621.3	612.7	623.7

The label “12” in the first row stands for the pair of images 1 and 2, and analogously for the other labels.



Fig. 10. Some images of the building.

### 6.3.2. An indoor scene

We took four images of a simple indoor scene as Fig. 11 shows. Interest points were mainly extracted on the three cups and just a few on the plug in the background, i.e., the scene is relatively “flat.”

The estimated focal lengths, for all 6 possible image pairs, are shown in Table 3. Again, the same camera setting as in Section 6.2 was used. The maximum relative error is about 6.5%, and the average relative error is less than 5%.



Fig. 11. Images of 3 cups.

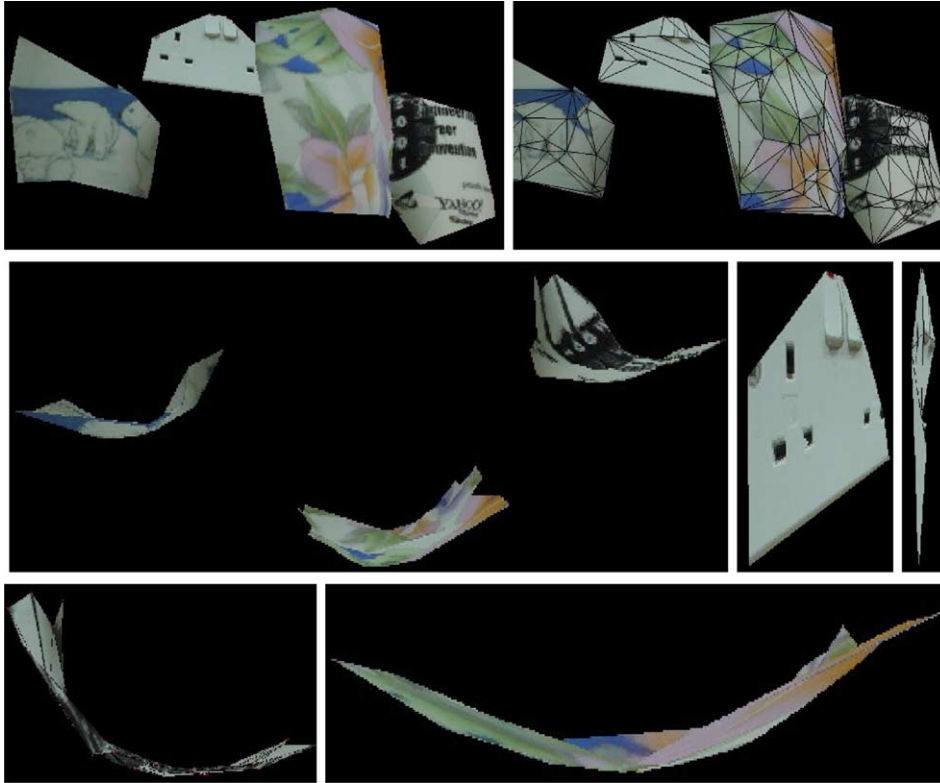


Fig. 12. Rendering of the reconstructed cup scene. (First row) General appearance of the scene, once with overlaid triangular mesh. (Second row) Rough top view of cups and two close-ups of the plug in the background (rightmost image shows the near coplanarity of the reconstruction). (Third row) Top views of two of the cups, showing that their cylindrical shape has been recovered.

As we did for the images of the calibration grid, we performed a 3D reconstruction of the scene using the calibration result. A triangular mesh is semi-automatically adjusted to the reconstructed 3D points, and used to create textured VRML models. A few renderings of one of the models are shown in Fig. 12. Due to the sparseness of the extracted interest points, the reconstruction of the scene is not complete. However, Fig. 12 shows that it is qualitatively correct, as explained in the caption of the figure.

## 7. Conclusions

We have analyzed the problem of focal length calibration from two views of an unknown scene, given their epipolar geometry and the assumption that the views have identical focal length. Closed form solutions have been derived, which

consist of one quadratic and two linear equations (which are algebraically interdependent). We have studied critical camera configurations in detail. Our experimental results suggest that in practice such configurations are relatively easy to avoid. Acceptably accurate results can be obtained when these singular configurations are avoided.

### Acknowledgment

Z.L. Cheng is very grateful for the scholarship granted by the National University of Singapore.

### Appendix A. Background

We describe a few known results about matrix decompositions that will be used in the following sections. Let the SVD of a  $3 \times 3$  matrix  $M$  of rank 2 be given as

$$M \stackrel{SVD}{=} U \Sigma V^T = (\mathbf{u}_1 \quad \mathbf{u}_2 \quad \mathbf{u}_3) \begin{pmatrix} \sigma_1 & 0 & 0 \\ 0 & \sigma_2 & 0 \\ 0 & 0 & 0 \end{pmatrix} \begin{pmatrix} \mathbf{v}_1^T \\ \mathbf{v}_2^T \\ \mathbf{v}_3^T \end{pmatrix}.$$

The right null-vectors of  $M$  are equal (up to scale) to the third column  $\mathbf{v}_3$  of  $V$ . As for the left null-vectors of  $M$ , they are equal (up to scale) to the third column  $\mathbf{u}_3$  of  $U$ .

In the following, we suppose that  $\sigma_1 \neq \sigma_2$ . Consider the symmetric matrix  $M^T M$ . It has 0,  $\sigma_1^2$ , and  $\sigma_2^2$  as eigenvalues. The eigenvectors of  $M^T M$  to the eigenvalue  $\sigma_i^2$  ( $i = 1, 2$ ) are equal (up to scale) to the  $i$ th column  $\mathbf{v}_i$  of  $V$ .

Similarly, the eigenvectors of  $MM^T$  to the eigenvalue  $\sigma_i^2$  ( $i = 1, 2$ ) are equal (up to scale) to the  $i$ th column  $\mathbf{u}_i$  of  $U$ .

### Appendix B. Parameterization of relative pose

In the following sections, we derive singular camera configurations. A geometric description is most useful. (Non-) Singularity only depends on the relative pose of the two views (and, in some very special cases, on the actual value of the focal length). Since only *relative* pose matters, we assume, without loss of generality, that the optical center of the first camera is the origin. Furthermore, we assume that its optical axis coincides with the  $Z$ -axis. Hence, the rotational part of its pose consists of a rotation  $R_{Z,1}$  about the  $Z$ -axis (cyclotorsion). This may, again without loss of generality, be chosen such that the optical center of the second camera lies in the plane  $X = 0$ , i.e., its coordinates are  $(0, Y, Z)$ . Without loss of generality, we may fur-

thermore impose that the distance between the two cameras is equal to 1. Hence, the second camera's position may be parameterized by an angle  $\gamma$

$$\begin{pmatrix} 0 \\ \cos \gamma \\ \sin \gamma \\ 1 \end{pmatrix}.$$

Let the second camera's orientation be given by three elementary rotation matrices:  $R_2 = R_{Z,2}R_YR_X$ . The semi-calibrated fundamental matrix for this parameterization is then given by

$$G \sim \begin{pmatrix} 1 & 0 & 0 \\ 0 & 1 & 0 \\ 0 & 0 & f \end{pmatrix} R_{Z,2}R_YR_X \left[ \begin{pmatrix} 0 \\ \cos \gamma \\ \sin \gamma \end{pmatrix} \right]_{\times} R_{Z,1} \begin{pmatrix} 1 & 0 & 0 \\ 0 & 1 & 0 \\ 0 & 0 & f \end{pmatrix}. \quad (\text{B.1})$$

Note that the rotations  $R_{Z,1}$  and  $R_{Z,2}$  have the following special form:

$$R_{Z,i} = \begin{pmatrix} \cdot & \cdot & 0 \\ \cdot & \cdot & 0 \\ 0 & 0 & 1 \end{pmatrix}$$

Hence, Eq. (B.1) can be rewritten as

$$G \sim R_{Z,2} \underbrace{\begin{pmatrix} 1 & 0 & 0 \\ 0 & 1 & 0 \\ 0 & 0 & f \end{pmatrix} R_YR_X \left[ \begin{pmatrix} 0 \\ \cos \gamma \\ \sin \gamma \end{pmatrix} \right]_{\times} \begin{pmatrix} 1 & 0 & 0 \\ 0 & 1 & 0 \\ 0 & 0 & f \end{pmatrix}}_H R_{Z,1}. \quad (\text{B.2})$$

Due to the special form of  $R_{Z,1}$  and  $R_{Z,2}$  and the orthogonality of the left and right singular matrices of an SVD,  $G$  and  $H$  have the same singular values and the third rows of their respective matrices  $U$  and  $V$  are equal to one another (up to sign at least). Specifically, this means that the SVDs of  $G$  and  $H$  lead to the same calibration equations.<sup>5</sup>

Hence, we may analyze the singularities of the calibration equations by studying the SVD of  $H$ , which allows us to express algebraic singularity conditions relatively easily in geometric terms, i.e., in terms of relative pose.

The matrix  $H$ , defined in (B.2) is given explicitly as

$$H \sim \begin{pmatrix} (\sin \gamma \sin \alpha - \cos \gamma \cos \alpha) \sin \beta & -\sin \gamma \cos \beta & f \cos \gamma \cos \beta \\ \sin \gamma \cos \alpha + \cos \gamma \sin \alpha & 0 & 0 \\ f(\sin \gamma \sin \alpha - \cos \gamma \cos \alpha) \cos \beta & f \sin \gamma \sin \beta & -f^2 \cos \gamma \sin \beta \end{pmatrix}. \quad (\text{B.3})$$

Here,  $\alpha$  and  $\beta$  are the angles of  $R_X$  and  $R_Y$ , respectively.

<sup>5</sup> In fact, this illustrates that cyclotorsion (rotation about the optical axis) does not influence focal length calibration.

In the following, we express conditions for coplanar or parallel optical axes, etc., in terms of the relative pose parameters  $\alpha$ ,  $\beta$ , and  $\gamma$ .

The *optical axis* of the second camera has the direction

$$\mathbf{D} \sim \begin{pmatrix} -\sin \beta \\ \sin \alpha \cos \beta \\ \cos \alpha \cos \beta \\ 0 \end{pmatrix}. \quad (\text{B.4})$$

Since the direction of the first optical axis is given by  $(0,0,1,0)^T$ , the optical axes are *parallel* exactly if

$$\sin \alpha = \sin \beta = 0. \quad (\text{B.5})$$

The two optical axes are *coplanar* exactly if  $H_{33} = 0$ , hence if  $\cos \gamma = 0$  or  $\sin \beta = 0$  (cf. Eq. (B.3)). The case  $\cos \gamma = 0$  means that the second camera's optical center lies on the first camera's optical axis.

Let us express these conditions in terms of the principal epipolar planes, defined in section 5. The two *principal epipolar planes* are computed as

$$\Pi_1 \sim \begin{pmatrix} \cos \gamma \\ 0 \\ 0 \\ 0 \end{pmatrix} \quad \Pi_2 \sim \begin{pmatrix} \cos \beta (\cos \alpha \cos \gamma - \sin \alpha \sin \gamma) \\ -\sin \beta \sin \gamma \\ \sin \beta \cos \gamma \\ 0 \end{pmatrix}.$$

The optical axes are coplanar if one or both principal epipolar planes are not defined (algebraically, if all their coefficients are zero) or if they are identical. Naturally, we find the same conditions as above: when  $\cos \gamma = 0$ ,  $\Pi_1$  is not defined (the second camera's optical center lies on the first optical axis). A necessary condition for  $\Pi_2$  not being defined is  $\sin \beta = 0$ . In that case, we observe that  $\Pi_1$  and  $\Pi_2$  are identical (their coordinate vectors are equal up to scale), thus the optical axes are coplanar.

Besides the different conditions for coplanar optical axes, another configuration is relevant: *mutually orthogonal principal epipolar planes* (cf. Section 5). This means that the scalar product of their normals (the upper 3-subvectors of  $\Pi_1$  and  $\Pi_2$ ) vanishes, which happens exactly if  $\Pi_{2,1} = 0$  (we exclude  $\cos \gamma = 0$  since  $\Pi_1$  is assumed to be defined):

$$\cos \beta (\cos \alpha \cos \gamma - \sin \alpha \sin \gamma) = 0.$$

Let us now consider the *equidistance configuration*: the optical axes are coplanar (but not parallel) and the optical centers are at the same distance from the intersection point of the optical axes. Let us develop this case for the two conditions of coplanar optical axes:

- $\cos \gamma = 0$ . In that case, the second optical center is the intersection point of the two optical axes, hence equidistance is excluded.

- $\sin \beta = 0$ . We exclude parallel optical axes, hence:  $\sin \alpha \neq 0$ . The intersection point of the optical axes is

$$\begin{pmatrix} 0 \\ 0 \\ \sin \gamma - \cos \gamma \frac{\cos \alpha}{\sin \alpha} \\ 1 \end{pmatrix}.$$

The squared distances to the optical centers are thus equal if

$$\frac{(\sin \gamma \sin \alpha - \cos \gamma \cos \alpha)^2}{\sin^2 \alpha} = \frac{\cos^2 \gamma}{\sin^2 \alpha}$$

which (since  $\sin \alpha \neq 0$ ) is equivalent to (after some trigonometric manipulations)

$$\sin \alpha (\cos^2 \gamma - \sin^2 \gamma) + 2 \cos \alpha \cos \gamma \sin \gamma = 0. \quad (\text{B.6})$$

The last case of interest is that of the angles between optical axes and baseline (line joining the optical centers) being equal. Note that this subsumes the equidistance configuration, but is more general. The condition for this case is given in the last row of the table.

All special cases of relative pose that are relevant in the following sections, are summarized in the table below.

#### Summary of relevant special cases for relative camera pose

Coplanar optical axes	$\cos \gamma = 0$ or $\sin \beta = 0$
2nd optical center on 1st optical axis	$\cos \gamma = 0$
1st optical center on 2nd optical axis	$\sin \beta = \cos \alpha \cos \gamma - \sin \alpha \sin \gamma = 0$
Parallel optical axes	$\sin \alpha = \sin \beta = 0$
Orthogonal principal epipolar planes	$\cos \beta (\cos \alpha \cos \gamma - \sin \alpha \sin \gamma) = 0$
Equidistance	$\sin \beta = \sin \alpha (\cos^2 \gamma - \sin^2 \gamma) + 2 \cos \alpha \cos \gamma \sin \gamma = 0$
Equal angles between optical axes and baseline	$\sin^2 \gamma = \cos^2 \beta (\sin \alpha \cos \gamma + \cos \alpha \sin \gamma)^2$

### Appendix C. Proofs for singularities of the calibration equations

Let us first define the meaning of singularity of the equations, based on observations made in Section 5: they are singular if all their coefficients vanish. In the following, we first derive conditions for singularity in terms of the elements of the SVD of  $G$ , respectively,  $H$ , concretely, in terms of the singular values  $a$  and  $b$  and the coefficients  $U_{31}$ ,  $U_{32}$ ,  $V_{31}$ , and  $V_{32}$  that show up in Eqs. (2)–(4). We then establish the corresponding geometrical configurations based on the proposed parameterization of relative pose.

The analysis of singularities is tricky due to the possibility that the SVD of the (semi-calibrated) fundamental matrix may not be unique. Note that the SVD is never

unique for any matrix: e.g., simultaneously scaling corresponding columns of  $U$  and  $V$  by  $-1$  gives another valid SVD. Such manipulations lead to the same calibration equations, as may be verified by checking Eqs. (2)–(4). Thus, in the following, we speak of *ambiguous SVD* if there are *infinitely many* possible SVDs for a matrix. In our case, this is exactly the case if  $H$  has two equal non-zero singular values  $a = b$ : if

$$H = U \begin{pmatrix} a & 0 & 0 \\ 0 & a & 0 \\ 0 & 0 & 0 \end{pmatrix} V^T$$

is an SVD of  $H$ , then also

$$H = \underbrace{U \begin{pmatrix} \cos \rho & \sin \rho & 0 \\ -\sin \rho & \cos \rho & 0 \\ 0 & 0 & 1 \end{pmatrix}}_{U'} \begin{pmatrix} a & 0 & 0 \\ 0 & a & 0 \\ 0 & 0 & 0 \end{pmatrix} \underbrace{\begin{pmatrix} \cos \rho & -\sin \rho & 0 \\ \sin \rho & \cos \rho & 0 \\ 0 & 0 & 1 \end{pmatrix}}_{V'^T} V^T$$

for any angle  $\rho$ .

In the following two sections, we first analyze the case of ambiguous SVDs, followed by that of a unique one.

## Appendix D. Singularities in the case of ambiguous SVDs

### D.1. Cases of ambiguous SVDs

In the following, we derive all cases in which the singular values of  $H$  are equal. The singular values of  $H$  are the square roots of the eigenvalues of  $H^T H$

$$H^T H \sim \begin{pmatrix} 1 & 0 & 0 \\ 0 & 1 & 0 \\ 0 & 0 & f \end{pmatrix} \left[ \begin{pmatrix} 0 \\ \cos \gamma \\ \sin \gamma \end{pmatrix} \right]_{\times} R_X^T R_Y^T \begin{pmatrix} 1 & 0 & 0 \\ 0 & 1 & 0 \\ 0 & 0 & f^2 \end{pmatrix} R_Y R_X \left[ \begin{pmatrix} 0 \\ \cos \gamma \\ \sin \gamma \end{pmatrix} \right]_{\times} \begin{pmatrix} 1 & 0 & 0 \\ 0 & 1 & 0 \\ 0 & 0 & f \end{pmatrix}.$$

We want to find the conditions for which  $H^T H$  has two equal non-zero eigenvalues (and one that is zero). In that case, its characteristic polynomial must be of the form

$$\lambda(\lambda - a)^2 = \lambda^3 - 2a\lambda^2 + a^2\lambda.$$

Hence, if we denote by  $x_i$  the coefficient of  $\lambda^i$ , we must have

$$4x_1 - x_2^2 = 0. \tag{D.1}$$

Let us formulate this condition for the characteristic polynomial of  $H^T H$ . In the following, we at times use the following compact notation:  $c_\alpha = \cos \alpha$  and  $s_\alpha = \sin \alpha$ , and analogously for other angles.

The expression in (D.1) can be factorized in three factors:

$$-(f^2 - 1)^2, \quad (\text{D.2})$$

$$(f^2 - 1)s_\beta^2 c_\gamma^2 + c_\gamma^2 + s_\beta^2 + c_\beta^2 (c_\alpha c_\gamma - s_\alpha s_\gamma)^2 + 2c_\beta c_\gamma (c_\alpha c_\gamma - s_\alpha s_\gamma), \quad (\text{D.3})$$

$$(f^2 - 1)s_\beta^2 c_\gamma^2 + c_\gamma^2 + s_\beta^2 + c_\beta^2 (c_\alpha c_\gamma - s_\alpha s_\gamma)^2 - 2c_\beta c_\gamma (c_\alpha c_\gamma - s_\alpha s_\gamma). \quad (\text{D.4})$$

If any one of the expressions (D.2)–(D.4) is equal to zero, then  $H^T H$  has two equal non-zero eigenvalues, and the SVD of  $H$  is not unique. The trivial case is obviously  $f^2 = 1$  (from Eq. (D.2)). This will be dealt with in detail in Section D.2.

As for  $f^2 \neq 1$ , we will show in the following that expressions (D.3) or (D.4) are equal to zero exactly in generic singular configurations. We consider three cases:  $c_\gamma = 0$ ,  $s_\beta = 0$ , and  $c_\gamma, s_\beta \neq 0$ .

- $c_\gamma = 0$ . The expressions in (D.3) and (D.4) are identical in this case:  $s_\beta^2 + c_\beta^2 s_\alpha^2$ . This is zero exactly if  $s_\alpha = s_\beta = 0$ . This means exactly, cf. the table in Appendix B, that the second camera lies on the optical axis of the first one ( $\cos \gamma = 0$ ) and that their optical axes are identical (since they are parallel, due to  $s_\alpha = s_\beta = 0$ ). Hence, we are in a special case of parallel optical axes, which is of course a generic degenerate situation.
- $s_\beta = 0$ . The expressions in (D.3) and (D.4) become (“+” for (D.3) and “–” for (D.4))

$$c_\gamma^2 + (c_\alpha c_\gamma - s_\alpha s_\gamma)^2 \pm 2c_\gamma (c_\alpha c_\gamma - s_\alpha s_\gamma) = (c_\gamma \pm (c_\alpha c_\gamma - s_\alpha s_\gamma))^2.$$

This is zero (for either “+” or “–”) exactly if

$$c_\gamma^2 = (c_\alpha c_\gamma - s_\alpha s_\gamma)^2.$$

Using trigonometric manipulations, this can be transformed into:

$$s_\alpha^2 \left( s_\gamma \left( c_\gamma^2 - s_\gamma^2 \right) + 2c_\alpha c_\gamma s_\gamma \right)^2 = 0.$$

This holds if  $s_\alpha = 0$  or  $s_\alpha (c_\gamma^2 - s_\gamma^2) + 2c_\alpha c_\gamma s_\gamma = 0$ . The first condition corresponds to parallel optical axes and the second one to the equidistance configuration, cf. the table in Appendix B. Hence, as above, the expressions (D.3) and (D.4) can only be zero (for  $f^2 \neq 1$ ) in generic degenerate situations.

- $c_\gamma, s_\beta \neq 0$ . We show in the following that under these assumptions, the expressions (D.3) and (D.4) cannot be zero for *positive* values of  $f^2$ . Expressions (D.3) or (D.4) being zero leads to (division by  $s_\beta^2 c_\gamma^2$  is allowed since this is assumed to be non-zero here)

$$f^2 = \frac{-s_\beta^2 s_\gamma^2 - c_\gamma^2 - c_\beta^2 (c_\alpha c_\gamma - s_\alpha s_\gamma)^2 \pm 2c_\beta c_\gamma (c_\alpha c_\gamma - s_\alpha s_\gamma)}{s_\beta^2 c_\gamma^2}.$$

Here, “+” corresponds to (D.3) and “–” to (D.4). We develop this equation:

$$f^2 = \frac{-s_\beta^2 s_\gamma^2 - (c_\gamma \mp c_\beta (c_\alpha c_\gamma - s_\alpha s_\gamma))^2}{s_\beta^2 c_\gamma^2}.$$

The right-hand side of this equation can obviously never be positive. Hence, the equation can never be true for real values of  $f$ , meaning that expressions (D.3) and (D.4) can not be zero (for  $f^2 \neq 1$  and under the assumption  $c_\gamma, s_\beta \neq 0$ ).

*Summary.* The semi-calibrated fundamental matrix has equal non-zero singular values exactly in the case  $f = \pm 1$  (expression (D.2)) or if the cameras are in equidistance configuration (includes the case of parallel optical axes). In the first case, the fundamental matrix is actually the essential matrix of the camera pair. In practice,  $f = \pm 1$  can happen if one works in standardized image coordinates [8] (which often comes down to scaling the images by approximately the inverse focal length), which is usually recommended for numerical reasons. As for the second case, equidistance, this represents a generic singularity, hence the calibration equations become singular anyway. In the following section, we thus only analyze the case  $f = \pm 1$ .

## D.2. The case $f = \pm 1$

In the following, we only consider the case  $f = +1$ ; as for  $f = -1$ , the equations are analogous, with only sign changes in appropriate places. The matrix  $H$  is now given by

$$H \sim R_Y R_X \begin{bmatrix} 0 \\ \cos \gamma \\ \sin \gamma \end{bmatrix}_\times.$$

As proven above,  $H$  has two equal singular values, i.e. its SVD is not unique. In practice, the SVD one obtains depends on the actual numerical implementation used to compute it. We want to investigate if our calibration equations may be singular for some SVDs and non-singular for others, or if they are (non-) singular irrespective of the actual SVD.

We write  $H$  in detail

$$\begin{aligned} H &\sim \begin{pmatrix} \cos \beta & 0 & \sin \beta \\ 0 & 1 & 0 \\ -\sin \beta & 0 & \cos \beta \end{pmatrix} \begin{pmatrix} 1 & 0 & 0 \\ 0 & \cos \alpha & -\sin \alpha \\ 0 & \sin \alpha & \cos \alpha \end{pmatrix} \begin{pmatrix} 0 & -\sin \gamma & \cos \gamma \\ \sin \gamma & 0 & 0 \\ -\cos \gamma & 0 & 0 \end{pmatrix} \\ &= \begin{pmatrix} \sin \beta (\sin \alpha \sin \gamma - \cos \alpha \cos \gamma) & -\cos \beta \sin \gamma & \cos \beta \cos \gamma \\ \cos \alpha \sin \gamma + \sin \alpha \cos \gamma & 0 & 0 \\ \cos \beta (\sin \alpha \sin \gamma - \cos \alpha \cos \gamma) & \sin \beta \sin \gamma & -\sin \beta \cos \gamma \end{pmatrix}. \end{aligned}$$

We now establish the possible SVDs of  $H$ . Since  $H$  is the product of two orthonormal matrices and another one, we can derive its SVDs from those of that other matrix. This is a skew-symmetric matrix, and all its SVDs can be shown to be of the following form, for some value of  $\rho$  (and up to changing signs for entire

columns or rows of the orthogonal matrices involved; this does not matter for our analysis):

$$\begin{aligned}
\begin{pmatrix} 0 & -s_\gamma & c_\gamma \\ s_\gamma & 0 & 0 \\ -c_\gamma & 0 & 0 \end{pmatrix} &\stackrel{SVD}{=} \begin{pmatrix} 0 & 1 & 0 \\ -s_\gamma & 0 & c_\gamma \\ c_\gamma & 0 & s_\gamma \end{pmatrix} \begin{pmatrix} c_\rho & s_\rho & 0 \\ -s_\rho & c_\rho & 0 \\ 0 & 0 & 1 \end{pmatrix} \begin{pmatrix} 1 & 0 & 0 \\ 0 & 1 & 0 \\ 0 & 0 & 0 \end{pmatrix} \\
&\times \begin{pmatrix} c_\rho & -s_\rho & 0 \\ s_\rho & c_\rho & 0 \\ 0 & 0 & 1 \end{pmatrix} \begin{pmatrix} -1 & 0 & 0 \\ 0 & -s_\gamma & c_\gamma \\ 0 & c_\gamma & s_\gamma \end{pmatrix} \\
&= \begin{pmatrix} -s_\rho & c_\rho & 0 \\ -c_\rho s_\gamma & -s_\rho s_\gamma & c_\gamma \\ c_\rho c_\gamma & s_\rho c_\gamma & s_\gamma \end{pmatrix} \begin{pmatrix} 1 & 0 & 0 \\ 0 & 1 & 0 \\ 0 & 0 & 0 \end{pmatrix} \begin{pmatrix} -c_\rho & s_\rho s_\gamma & -s_\rho c_\gamma \\ -s_\rho & -c_\rho s_\gamma & c_\rho c_\gamma \\ 0 & c_\gamma & s_\gamma \end{pmatrix},
\end{aligned}$$

where we use, as above, the shorthand notation  $c_\alpha = \cos \alpha$  and  $s_\alpha = \sin \alpha$ , and analogously for other angles.

Hence, the SVDs of  $H$  are parameterized by the same angle  $\rho$ , and are of the following form:

$$\underbrace{\begin{pmatrix} -s_\rho & c_\rho & 0 \\ -c_\rho s_\gamma & -s_\rho s_\gamma & c_\gamma \\ c_\rho c_\gamma & s_\rho c_\gamma & s_\gamma \end{pmatrix}}_U \begin{pmatrix} 1 & 0 & 0 \\ 0 & 1 & 0 \\ 0 & 0 & 0 \end{pmatrix} \underbrace{\begin{pmatrix} -c_\rho & s_\rho s_\gamma & -s_\rho c_\gamma \\ -s_\rho & -c_\rho s_\gamma & c_\rho c_\gamma \\ 0 & c_\gamma & s_\gamma \end{pmatrix}}_{V^T}$$

with  $U$  explicitly of the form:

$$U = \begin{pmatrix} c_\beta & 0 & s_\beta \\ 0 & 1 & 0 \\ -s_\beta & 0 & c_\beta \end{pmatrix} \begin{pmatrix} 1 & 0 & 0 \\ 0 & c_\alpha & -s_\alpha \\ 0 & s_\alpha & c_\alpha \end{pmatrix} \begin{pmatrix} -s_\rho & c_\rho & 0 \\ -c_\rho s_\gamma & -s_\rho s_\gamma & c_\gamma \\ c_\rho c_\gamma & s_\rho c_\gamma & s_\gamma \end{pmatrix}.$$

Let us call  $X = c_\beta(c_\alpha c_\gamma - s_\alpha s_\gamma)$ . From the above SVD, we identify the values used in the calibration equations:

$$a = b,$$

$$U_{31} = s_\beta s_\rho + c_\rho X,$$

$$U_{32} = -s_\beta c_\rho + s_\rho X,$$

$$V_{31} = -s_\rho c_\gamma,$$

$$V_{32} = c_\rho c_\gamma.$$

Note that  $X = 0$  is the condition for orthogonal principal epipolar planes (cf. the table in Appendix B). Let us further define:

$$Y = U_{31}^2 V_{31}^2 - U_{32}^2 V_{32}^2,$$

$$Z = U_{32}^2 - U_{31}^2 + V_{32}^2 - V_{31}^2.$$

The quadratic equation can now be written as (we factor out  $a = b$ ):

$$f^4(Y + Z) - f^2(2Y + Z) + Y = 0.$$

Its coefficients vanish all exactly if  $Y = Z = 0$ . Let us go into details (we use the relationship  $s_\rho^4 - c_\rho^4 = s_\rho^2 - c_\rho^2$ ):

$$Y = U_{31}^2 V_{31}^2 - U_{32}^2 V_{32}^2 = s_\beta c_\gamma^2 (2c_\rho s_\rho X + s_\beta (s_\rho^2 - c_\rho^2)) = 0, \quad (\text{D.5})$$

$$Z = U_{32}^2 - U_{31}^2 + V_{32}^2 - V_{31}^2 = -4c_\rho s_\rho s_\beta X + (s_\beta^2 + c_\gamma^2 - X^2)(c_\rho^2 - s_\rho^2) = 0. \quad (\text{D.6})$$

In the following, we consider two questions:

- for which relative camera poses do (D.5) and (D.6) hold *whatever* value  $\rho$  has?
- do values for  $\rho$  exist for any relative camera pose, such that (D.5) and (D.6) hold?

#### D.2.1. Relative camera poses for which (D.5) and (D.6) hold for every $\rho$

Let us consider any value of  $\rho$  different from 0. Dividing (D.5) and (D.6) by  $c_\rho^2$  gives:

$$t_\rho^2 (s_\beta^2 c_\gamma^2) + 2t_\rho (s_\beta c_\gamma^2 X) - s_\beta^2 c_\gamma^2 = 0,$$

$$t_\rho^2 (X^2 - s_\beta^2 - c_\gamma^2) - 4t_\rho (s_\beta X) + (s_\beta^2 + c_\gamma^2 - X^2) = 0,$$

where  $t_\rho = \tan \rho$ . The equations hold for every value of  $\rho$  exactly if the coefficients of powers of  $t_\rho$  all vanish, hence if all the following equations hold (we leave out the ones occurring twice):

$$s_\beta^2 c_\gamma^2 = 0,$$

$$s_\beta c_\gamma^2 X = 0,$$

$$X^2 - s_\beta^2 - c_\gamma^2 = 0,$$

$$s_\beta X = 0.$$

If  $s_\beta = 0$ , then the third equation holds if  $X^2 - c_\gamma^2 = 0$  (we will examine this case just below). If  $s_\beta \neq 0$ , then the first and fourth equation imply that  $c_\gamma = X = 0$ . In that case, however, the third equation would not be satisfied. Hence, the only possible case is  $s_\beta = X^2 - c_\gamma^2 = 0$ . Let us examine it in detail.

The term  $X^2 - c_\gamma^2$  can be expanded as follows:

$$\begin{aligned} -c_\gamma^2 + (c_\alpha c_\gamma - s_\alpha s_\gamma)^2 &= c_\gamma^2 (c_\alpha^2 - 1) + s_\gamma^2 s_\alpha^2 - 2c_\alpha s_\alpha c_\gamma s_\gamma \\ &= (s_\gamma^2 - c_\gamma^2) s_\alpha^2 - 2c_\alpha s_\alpha c_\gamma s_\gamma \\ &= s_\alpha \left( (s_\gamma^2 - c_\gamma^2) s_\alpha - 2c_\alpha c_\gamma s_\gamma \right). \end{aligned}$$

It is equal to zero if  $s_x = 0$  or if  $(s_\gamma^2 - c_\gamma^2)s_x - 2c_x c_\gamma s_\gamma = 0$ . The first case, together with the assumption  $s_\beta = 0$ , corresponds to the case of parallel optical axes (cf. the table in Appendix B). The second case, corresponds to the equidistance condition. Hence, both cases correspond to generic singular configurations.

We conclude that for  $f = \pm 1$ , the quadratic calibration vanishes *whichever* SVD one happens to compute (whatever value  $\rho$  has) only in the generic singular configurations.

#### D.2.2. For which relative camera poses can (D.5) and (D.6) hold?

Note that in the following, only generic non-singular configurations are of interest. Let us now consider the question for different cases:

- $\sin \beta = 0$ . Eq. (D.5) holds and (D.6) becomes

$$(c_\gamma^2 - X^2)(c_\rho^2 - s_\rho^2) = 0.$$

As shown in Section D.2.1, the first possibility,  $c_\gamma^2 - X^2 = 0$ , corresponds to generic singular configurations, hence is not of interest here. As for the second possibility,  $c_\rho^2 - s_\rho^2 = 0$ , it tells us that for all relative camera poses with  $\sin \beta = 0$ , there exist four different values for  $\rho$  (separated by  $90^\circ$ ), for which the quadratic calibration equation vanishes.

- $\sin \beta \neq 0$ ,  $\cos \gamma = 0$ ,  $\sin^2 \beta - \cos^2 \beta \sin^2 \alpha = 0$ . Eq. (D.5) holds and (D.6) becomes

$$c_\rho s_\rho c_\beta s_\beta s_x = 0.$$

Hence, for all relative camera poses corresponding to the assumptions made here, there again exist four different values for  $\rho$  (separated by  $90^\circ$ ), for which the quadratic calibration equation vanishes.

- $\sin \beta \neq 0$ ,  $\cos \gamma = 0$ ,  $\sin^2 \beta - \cos^2 \beta \sin^2 \alpha \neq 0$ . Eq. (D.5) holds and (D.6) becomes (the  $\pm$  corresponds to  $\sin \gamma = \pm 1$ )

$$\pm 4c_\rho s_\rho c_\beta s_\beta s_x + (s_\beta^2 - c_\beta^2 s_x^2)(c_\rho^2 - s_\rho^2) = 0.$$

Let us first note that for  $c_\rho = 0$ , this equation cannot hold, due to the assumption that  $s_\beta^2 - c_\beta^2 s_x^2 \neq 0$ . We may thus divide the equation by  $c_\rho^2$ . After some modifications, this leads to:

$$t_\rho^2 (c_\beta^2 s_x^2 - s_\beta^2) \pm 4t_\rho c_\beta s_\beta s_x - (c_\beta^2 s_x^2 - s_\beta^2) = 0.$$

It is easy to verify that, whatever values  $\alpha$  and  $\beta$  have (if compatible with the assumptions made here), there exist exactly two solutions for  $t_\rho = \tan \rho$ . Hence, for all relative camera poses corresponding to the assumptions made here, there again exist four different values for  $\rho$  (separated by  $90^\circ$ ), for which the quadratic calibration equation vanishes.

Hence, for all relative camera poses corresponding to the assumptions made here, there again exist four different values for  $\rho$ , for which the quadratic calibration equation vanishes.

- $\sin \beta \neq 0$ ,  $\cos \gamma \neq 0$ . For (D.5) to hold, we must have

$$2c_\rho s_\rho X + s_\beta (s_\rho^2 - c_\rho^2) = 0.$$

Multiplying this equation with  $2s_\beta$  and adding this to (D.6) gives a *necessary* condition for the vanishing of the quadratic calibration equation

$$(-s_\beta^2 + c_\gamma^2 - X^2)(c_\rho^2 - s_\rho^2) = 0.$$

It is easy to verify that  $(-s_\beta^2 + c_\gamma^2 - X^2) = 0$  is equivalent to the condition of equal angles between optical axes and baseline (cf. the table in Appendix B) and that under the assumption  $\sin \beta \neq 0$ ,  $\cos \gamma \neq 0$ , there exist four different values for  $\rho$  for which (D.5) and (D.6) hold.

As for  $(-s_\beta^2 + c_\gamma^2 - X^2) \neq 0$ , the necessary condition is  $c_\rho^2 - s_\rho^2 = 0$ . Substituting this into (D.5) and (D.6), leads to the condition  $s_\beta c_\gamma^2 X = 0$ . Since here we assume that  $\sin \beta \neq 0$  and  $\cos \gamma \neq 0$ , we thus conclude that for  $X = 0$  (orthogonal principal epipolar planes, see above), four different values for  $\rho$  exist (due to  $c_\rho^2 - s_\rho^2 = 0$ ), for which the quadratic calibration equation vanishes.

### D.2.3. Summary

The quadratic equation vanishes of course in generic degenerate conditions. The only other case where it may vanish is when  $f = \pm 1$ . This may happen because the SVD of the fundamental matrix is ambiguous. For  $f = \pm 1$ , the coefficients of the quadratic equation may all be zero, depending on which SVD one happens to compute in practice (which angle  $\rho$ ). This can happen in exactly the following non-generic singular configurations: (i) the optical axes are coplanar, (ii) the principal epipolar planes are mutually orthogonal, or (iii) the angles between the optical axes and the baseline, are equal. In each of these cases, only four different values of  $\rho$  (four among the infinitely many ambiguous SVDs) exist for which the quadratic calibration equation vanishes. Hence, the chances for the quadratic equation to vanish in generical non-singular configurations, are small. Nevertheless, instabilities may indeed occur in cases close to  $f = \pm 1$ , i.e., when working in nearly perfectly standardized coordinates, as illustrated in Section 6.1.4.

## Appendix E. Singularities in the case of a unique SVD

We now consider the cases where the semi-calibrated fundamental matrix has a unique SVD (up to switching entire columns or rows or changing signs for entire columns or rows), i.e., different non-zero singular values  $a$  and  $b$ .

### E.1. Quadratic equation

Zeroing the three coefficients of Eq. (4) leads to the following equations:

$$a^2(1 - U_{31}^2 - V_{31}^2 + U_{31}^2 V_{31}^2) = b^2(1 - U_{32}^2 - V_{32}^2 + U_{32}^2 V_{32}^2), \quad (\text{E.1})$$

$$a^2(U_{31}^2 + V_{31}^2 - 2U_{31}^2 V_{31}^2) = b^2(U_{32}^2 + V_{32}^2 - 2U_{32}^2 V_{32}^2), \quad (\text{E.2})$$

$$a^2 U_{31}^2 V_{31}^2 = b^2 U_{32}^2 V_{32}^2. \quad (\text{E.3})$$

Substituting (E.3) into (E.1) and (E.2), we get:

$$a^2(1 - U_{31}^2 - V_{31}^2) = b^2(1 - U_{32}^2 - V_{32}^2), \quad (\text{E.4})$$

$$a^2(U_{31}^2 + V_{31}^2) = b^2(U_{32}^2 + V_{32}^2). \quad (\text{E.5})$$

Adding these two equations together, leads to  $a^2 = b^2$ . This is in contradiction with our assumptions (unique SVD). We conclude that the quadratic equation is never degenerate when the SVD is unique, i.e., when the cameras are not in an equidistance configuration (including parallel optical axes) and if  $f \neq \pm 1$ .

Further below, we examine special cases where one of its coefficients vanishes, and especially a case where the quadratic equation becomes linear.

### E.2. Linear equations

It is easy to show that *both* linear equations degenerate if any one of the following conditions holds:

$$U_{32} = V_{31} = 0, \quad (\text{E.6})$$

$$U_{32} = V_{32} = 0, \quad (\text{E.7})$$

$$U_{31} = V_{31} = 0, \quad (\text{E.8})$$

$$U_{31} = V_{32} = 0. \quad (\text{E.9})$$

The only other singularities occur, for Eq. (2), if

$$V_{31} = \pm U_{32} \quad \text{and} \quad aU_{31} = \mp bV_{32} \quad (\text{E.10})$$

and, for Eq. (3), if

$$V_{32} = \pm U_{31} \quad \text{and} \quad aV_{31} = \mp bU_{32}. \quad (\text{E.11})$$

Any one of the conditions (E.6), (E.9), (E.10), and (E.11) implies that the optical axes are coplanar (they imply that  $H_{33} = 0$ , cf. Appendix B). Only the conditions (E.7) and (E.8) may correspond to non-coplanar optical axes. In the following section, we consider the case of coplanar optical axes, and show that this always implies the degeneracy of the linear equations. We then consider the case of non-coplanar axes and examine cases where the linear equations degenerate.

### E.3. Coplanar optical axes

As shown in Appendix B, the optical axes are coplanar if  $\cos \gamma = 0$  or  $\sin \beta = 0$ . We examine the two cases in the following.

### E.3.1. $\cos \gamma = 0$

This means that the optical center of the second camera is the point  $(0, 0, \sin \gamma, 1)$ , i.e., it lies on the optical axis of the first camera (the  $Z$ -axis). In this case, the first epipole has coordinates  $(0, 0, 1)^T$ . Since the first epipole is the null-vector of the fundamental matrix  $H$ , it is equal (up to sign) to the third *column*  $\mathbf{v}_3$  of the matrix  $V$  in its SVD. Due to the orthogonality of  $V$ , this implies that its third *row* is also given as  $(0, 0, \pm 1)$ , hence we have:  $V_{31} = V_{32} = 0$ . Hence, the quadratic equation (4) becomes

$$f^2 \{ f^2 (a^2 (1 - U_{31}^2) - b^2 (1 - U_{32}^2)) + (a^2 U_{31}^2 - b^2 U_{32}^2) \} = 0.$$

The spurious solution of that equation is  $f = 0$ , and can thus be always rejected, meaning the quadratic equation gives a unique admissible solution.

Consider now the symmetric matrix  $HH^T = U \text{diag}(a^2, b^2, 0)U^T$ . The columns of  $U$  are the eigenvectors of  $HH^T$ . It can be shown that

$$\begin{pmatrix} \sin \alpha \\ \cos \alpha \sin \beta \\ 0 \end{pmatrix}$$

is an eigenvector of  $HH^T$  to a non-zero eigenvalue (thus,  $a^2$  or  $b^2$ ). Hence, this vector must be equal (up to scale) to one of the first two columns of  $U$ , which means that  $U_{31} = 0$  or  $U_{32} = 0$ . Together with the condition  $V_{31} = V_{32} = 0$  shown above, this implies that at least one of (E.6)–(E.9) is true, hence both linear equations, (2) and (3), are degenerate.

### E.3.2. $\sin \beta = 0$

In this case, both  $H^T H$  and  $HH^T$  have  $(1, 0, 0)^T$  as an eigenvector with non-zero eigenvalue. Hence, one of the first two columns of  $U$  and one of first two columns of  $V$  have this form. It can be shown that if the first column of  $U$  has that form, then the second column of  $V$  is of the same form, and vice versa. This means that either  $U_{31} = V_{32} = 0$  or  $U_{32} = V_{31} = 0$ , which implies that both linear equations vanish and that the quadratic one becomes

$$f^2 \{ f^2 (a^2 (1 - U_{31}^2) - b^2 (1 - V_{32}^2)) + (a^2 U_{31}^2 - b^2 V_{32}^2) \} = 0 \quad (\text{E.12})$$

if  $U_{32} = V_{31} = 0$  or

$$f^2 \{ f^2 (a^2 (1 - V_{31}^2) - b^2 (1 - U_{32}^2)) + (a^2 V_{31}^2 - b^2 U_{32}^2) \} = 0 \quad (\text{E.13})$$

if  $U_{31} = V_{32} = 0$ . Hence, as in Section E.3.1, the quadratic equation gives a single admissible solution.

### E.3.3. Summary

Whenever the optical axes are coplanar, the two linear equations (2) and (3) vanish and the quadratic equation (4) gives in general a single admissible solution. The latter one vanishes completely exactly in the equidistance configuration (including parallel optical axes). Hence all singular cases of the quadratic equation in the coplanar case are generic singular cases, with the exception of the special cases for  $f = \pm 1$ .

## Appendix F. Non-coplanar optical axes

### F.1. Linear equations

As Section E.2 shows, the singular cases for non-coplanar optical axes are, for the linear equations, given by Eqs. (E.7) and (E.8):

$$U_{32} = V_{32} = 0,$$

$$U_{31} = V_{31} = 0.$$

#### F.1.1. First case: $U_{32} = V_{32} = 0$

In the following, the SVD of  $H$  is considered. The right null-vector (first epipole) of  $H$  is easily seen to be  $(0, f \cos \gamma, \sin \gamma)^T$  (cf. Eq. (B.3)). As described in Appendix A, this vector is equal, up to scale, to the third column  $\mathbf{v}_3$  of  $V$ . Hence we have<sup>6</sup>:

$$\begin{aligned} H &\sim \begin{pmatrix} (\sin \gamma \sin \alpha - \cos \gamma \cos \alpha) \sin \beta & -\sin \gamma \cos \beta & f \cos \gamma \cos \beta \\ \sin \gamma \cos \alpha + \cos \gamma \sin \alpha & 0 & 0 \\ f(\sin \gamma \sin \alpha - \cos \gamma \cos \alpha) \cos \beta & f \sin \gamma \sin \beta & -f^2 \cos \gamma \sin \beta \end{pmatrix} \\ &\sim \underbrace{\begin{pmatrix} U_{11} & U_{12} & U_{13} \\ U_{21} & U_{22} & U_{23} \\ U_{31} & 0 & U_{33} \end{pmatrix}}_U \begin{pmatrix} a & 0 & 0 \\ 0 & b & 0 \\ 0 & 0 & 0 \end{pmatrix} \underbrace{\begin{pmatrix} V_{11} & V_{21} & V_{31} \\ V_{12} & V_{22} & 0 \\ 0 & f \cos \gamma & \sin \gamma \end{pmatrix}}_{V^T}. \end{aligned} \quad (\text{F.1})$$

From the orthogonality of rows 2 and 3 of  $V^T$ , it follows that  $V_{22} = 0$  and from this, that  $V_{11} = 0$ . From  $H_{22} = H_{23} = 0$ , it also follows that  $U_{21} = 0$ . Hence (F.1) is rewritten as

$$\begin{aligned} &\begin{pmatrix} (\sin \gamma \sin \alpha - \cos \gamma \cos \alpha) \sin \beta & -\sin \gamma \cos \beta & f \cos \gamma \cos \beta \\ \sin \gamma \cos \alpha + \cos \gamma \sin \alpha & 0 & 0 \\ f(\sin \gamma \sin \alpha - \cos \gamma \cos \alpha) \cos \beta & f \sin \gamma \sin \beta & -f^2 \cos \gamma \sin \beta \end{pmatrix} \\ &\sim \begin{pmatrix} U_{11} & U_{12} & U_{13} \\ 0 & U_{22} & U_{23} \\ U_{31} & 0 & U_{33} \end{pmatrix} \begin{pmatrix} a & 0 & 0 \\ 0 & b & 0 \\ 0 & 0 & 0 \end{pmatrix} \begin{pmatrix} 0 & V_{21} & V_{31} \\ V_{12} & 0 & 0 \\ 0 & f \cos \gamma & \sin \gamma \end{pmatrix} \\ &= \begin{pmatrix} bU_{12}V_{12} & aU_{11}V_{21} & aU_{11}V_{31} \\ bU_{22}V_{12} & 0 & 0 \\ 0 & aU_{31}V_{21} & aU_{31}V_{31} \end{pmatrix}. \end{aligned}$$

From the coefficient (3,1) of that equation, we derive

<sup>6</sup> Here unitary determinant of the orthogonal matrix  $V$  is not imposed.

$$(\sin \gamma \sin \alpha - \cos \gamma \cos \alpha) \cos \beta = 0$$

which is thus a necessary condition for non-coplanar singular cases for the linear equations in the first case. Note that this condition is nothing else than that for mutually orthogonal principal epipolar planes, cf. the table in Appendix B.

In the following it is shown that this condition is also a sufficient one. We do this by giving analytical SVDs<sup>7</sup> for H in the two cases  $\cos \beta = 0$  and  $\sin \gamma \sin \alpha - \cos \gamma \cos \alpha = 0$ . Based on these SVDs, the coefficients of the linear calibration Eqs. (2) and (3) can be computed and it will be seen that they all vanish.

- $\cos \beta = 0$ . This implies that  $\sin \beta = \pm 1$  and H becomes

$$H \sim \begin{pmatrix} \pm \sin \gamma \sin \alpha \mp \cos \gamma \cos \alpha & 0 & 0 \\ \sin \gamma \cos \alpha + \cos \gamma \sin \alpha & 0 & 0 \\ 0 & \pm f \sin \gamma & \mp f^2 \cos \gamma \end{pmatrix}. \quad (\text{F.2})$$

Its SVD is given by (using the same shorthand notation as further above)

$$\underbrace{\begin{pmatrix} 0 & \pm s_x s_\gamma \mp c_x c_\gamma & \pm c_x s_\gamma \pm s_x c_\gamma \\ 0 & c_x s_\gamma + s_x c_\gamma & c_x c_\gamma - s_x s_\gamma \\ 1 & 0 & 0 \end{pmatrix}}_U \begin{pmatrix} f t_2 & 0 & 0 \\ 0 & 1 & 0 \\ 0 & 0 & 0 \end{pmatrix} \underbrace{\begin{pmatrix} 0 & \pm s_\gamma & \mp f c_\gamma \\ t_2 & 0 & 0 \\ 0 & f c_\gamma & s_\gamma \end{pmatrix}}_{V^T}, \quad (\text{F.3})$$

where  $t_2 = \sqrt{f^2 \cos^2 \gamma + \sin^2 \gamma}$ . It is easy to verify that (F.3) indeed is an SVD of H: the matrices U and V are orthonogonal and the product of the above expression equals H, as given in (F.2).

We thus have  $U_{32} = V_{32} = 0$ , which was already shown in Section E.2 to be a sufficient condition for degeneracy of the linear equations.

- $\sin \gamma \sin \alpha - \cos \gamma \cos \alpha = 0$ . Note that in this case, we have  $\cos \gamma \neq 0$  and  $\sin \alpha \neq 0$ : the condition  $\cos \gamma = 0$  can be excluded since it would imply coplanar optical axes (cf. Appendix B). Concerning  $\sin \alpha \neq 0$ : if  $\sin \alpha = 0$ , then  $\cos \alpha = \pm 1$  and  $\sin \gamma \sin \alpha - \cos \gamma \cos \alpha = \mp \cos \gamma \neq 0$ , which is contradictory to our assumption here. We may thus put:

$$\sin \gamma = \frac{\cos \alpha}{\sin \alpha} \cos \gamma.$$

H becomes

$$H \sim \begin{pmatrix} 0 & -s_\gamma c_\beta & f c_\gamma c_\beta \\ s_\gamma c_\alpha + c_\gamma s_\alpha & 0 & 0 \\ 0 & f s_\gamma s_\beta & -f^2 c_\gamma s_\beta \end{pmatrix} \sim \begin{pmatrix} 0 & -c_x c_\beta & f s_x c_\beta \\ 1 & 0 & 0 \\ 0 & f c_x s_\beta & -f^2 s_x s_\beta \end{pmatrix}.$$

An SVD for H is given by:

<sup>7</sup> The analytical SVDs in this section are given up to possible switching of columns of the involved matrices and, for easier expressions, up to scale for the orthogonal matrices U and V.

$$\begin{pmatrix} \cos \beta & 0 & f \sin \beta \\ 0 & t_2 & 0 \\ -f \sin \beta & 0 & \cos \beta \end{pmatrix} \begin{pmatrix} t_1 t_2 & 0 & 0 \\ 0 & 1 & 0 \\ 0 & 0 & 0 \end{pmatrix} \begin{pmatrix} 0 & -\cos \alpha & f \sin \alpha \\ t_1 & 0 & 0 \\ 0 & f \sin \alpha & \cos \alpha \end{pmatrix} \quad (\text{F.4})$$

with  $t_1 = \sqrt{f^2 \sin^2 \alpha + \cos^2 \alpha}$  and  $t_2 = \sqrt{f^2 \sin^2 \beta + \cos^2 \beta}$ . Again, we have  $U_{32} = V_{32} = 0$ , meaning that the linear calibration equations degenerate.

### F.1.2. Second case: $U_{31} = V_{31} = 0$

The analysis can be done analogously as above, leading to the same conclusions (the SVDs are the same, up to swapping of the singular values and corresponding columns of  $U$  and  $V$ ). Which one of the cases  $U_{32} = V_{32} = 0$  or  $U_{31} = V_{31} = 0$  occurs in practice, depends on which one of the singular values is larger.

## F.2. Quadratic equation

If we exclude  $f = \pm 1$ , then non-coplanar optical axes imply that  $a \neq b$  (follows from Section D.1) and hence the quadratic equation is non-degenerate. We now consider what happens in the cases where the linear equations degenerate:  $\cos \beta = 0$  or  $\sin \gamma \sin \alpha - \cos \gamma \cos \alpha = 0$ , cf. Section F.1.1.

- $\cos \beta = 0$ . The SVD of  $H$  in this case is given in Eq. (F.3). We substitute its coefficients in the quadratic equation, and get

$$-g^4 + g^2 f^2 \sin^2 \gamma + f^4 \cos^2 \gamma = 0,$$

where  $f$  is the true focal length and  $g$  the estimated one. Its two solutions are  $g^2 = f^2$  and  $g^2 = -f^2 \cos^2 \gamma$ . Being always negative (or zero), the second solution can be ruled out, which means that the quadratic equation gives a unique feasible solution here.

- $\sin \gamma \sin \alpha - \cos \gamma \cos \alpha = 0$ . Substituting the coefficients of the SVD of  $H$ , given in Eq. (F.4), in the quadratic equation, we get

$$g^4 (\cos^2 \alpha \cos^2 \beta - 1) + g^2 f^2 (\cos^2 \alpha \sin^2 \beta + \sin^2 \alpha \cos^2 \beta) + f^4 \sin^2 \alpha \sin^2 \beta = 0.$$

Besides  $f^2$ ,  $g^2$  has the following solution:

$$-\frac{\sin^2 \alpha \sin^2 \beta}{\sin^2 \beta + \sin^2 \alpha \cos^2 \beta}$$

which is always non-positive.<sup>8</sup> Hence, the quadratic equation has again a unique admissible solution.

<sup>8</sup> Note that the denominator is assured not to be zero, since we exclude  $\sin \beta = 0$  (we consider non-coplanar optical axes) and  $\sin \alpha = 0$  (cf. Section F.1.1).

### F.3. Summary

If the optical axes are non-coplanar, then the quadratic equation is never degenerate (with the exception of the special case  $f = \pm 1$  discussed in Section D.2). In addition, in all cases where the linear equations vanish, the spurious solution of the quadratic equation can be ruled out due to being non-positive.

### References

- [1] S. Bougnoux, From projective to Euclidean space under any practical situation, a criticism of self-calibration, in: Proc. 6th Internat. Conf. on Computer Vision, Bombay, India, January, 1998, pp. 790–796.
- [2] M. Brooks, L. De Agapito, D. Huynh, L. Baumela, Towards robust metric reconstruction via a dynamic uncalibrated stereo head, *Image Vision Comput.* 16 (14) (1998) 989–1002.
- [3] O. Faugeras, O. Luong, S. Maybank, Camera self-calibration: theory and experiments, in: Proc. European Conf. on Computer Vision LNCS, vol. 588, Springer-Verlag, Berlin, 1992, pp. 321–334.
- [4] O. Faugeras, Q.-T. Luong, *The Geometry of Multiple Images*, MIT Press, Cambridge, 2001.
- [5] G.H. Golub, C.F. van Loan, *Matrix computation*, The Johns Hopkins University Press, 1989.
- [6] R. Hartley, Estimation of relative camera positions for uncalibrated cameras, in: Proc. Eur. Conf. on Computer Vision, 1992, pp. 579–587.
- [7] R. Hartley, In defence of the 8-point algorithm, in: Proc. 5th Internat. Conf. on Computer Vision, Boston, USA, 1995, pp. 1064–1070.
- [8] R. Hartley, Kruppa’s equations derived from the fundamental matrix, *IEEE Trans. Pattern Anal. Mach. Intell.* 19 (2) (1997) 133–135.
- [9] R. Hartley, P. Sturm, Triangulation, *Comput. Vision Image Understand.* 68 (2) (1997) 146–157.
- [10] R. Hartley, A. Zisserman, *Multiple View Geometry in Computer Vision*, Cambridge University Press, Cambridge, 2000.
- [11] A. Heyden, K. Åström, Euclidean reconstruction from image sequences with varying and unknown focal length and principal point, in: Proc. IEEE Conf. on Computer Vision and Pattern Recognition, 1997, pp. 438–443.
- [12] F. Kahl, B. Triggs, Critical motions in Euclidean structure from motion, in: Proc. IEEE Conf. on Computer Vision and Pattern Recognition, vol. 2, 1999, pp. 366–372.
- [13] F. Kahl, B. Triggs, K. Åström, Critical motions for auto-calibration when some intrinsic parameters can vary, *J. Math. Imaging Vision* 13 (2) (2000) 131–146.
- [14] G.N. Newsam, D.Q. Huynh, M.J. Brooks, H.P. Pan, Recovering unknown focal lengths in self-calibration: an essentially linear algorithm and degenerate configurations, *ISPRS-Congress XXXI (B3)* (1996) 575–580.
- [15] M. Pollefeys, R. Koch, L. Van Gool, Self-calibration and metric reconstruction in spite of varying and unknown internal camera parameters, in: Proc. 6th Internat. Conf. on Computer Vision, Bombay, India, 1998, pp. 90–96.
- [16] M. Pollefeys, Self-calibration and metric 3D reconstruction from uncalibrated image sequences. PhD Thesis, Katholieke Universiteit Leuven, Belgium, 1999.
- [17] P. Sturm, Critical motion sequences for monocular self-calibration and uncalibrated Euclidean reconstruction, in: Proc. IEEE Conf. on Computer Vision and Pattern Recognition, Puerto Rico, June, 1997, pp. 1100–1105.
- [18] P. Sturm, A case against Kruppa’s equations for camera self-calibration, *IEEE Trans. Pattern Anal. Mach. Intell.* 22 (10) (2000) 1199–1204.
- [19] P. Sturm, On focal length calibration from two views, in: Proc. IEEE Conf. on Computer Vision and Pattern Recognition, Kauai, 2001, pp. 145–150.
- [20] P. Sturm, Critical motion sequences for the self-calibration of cameras and stereo systems with variable focal length, *Image Vision Comput.* 20 (5–6) (2002) 415–426.

- [21] Z. Zhang, R. Deriche, O. Faugeras, Q. Luong, A robust technique for matching two uncalibrated images through the recovery of the unknown epipolar geometry, *Artif. Intell.* 78 (1995) 87–119.
- [22] C. Zeller, O. Faugeras, Camera self-calibration from video sequences: the Kruppa equations revisited. Rapport de Recherche 2793, INRIA, France, 1996.